The Swiss -Norwegian Beam Lines
at ESRF

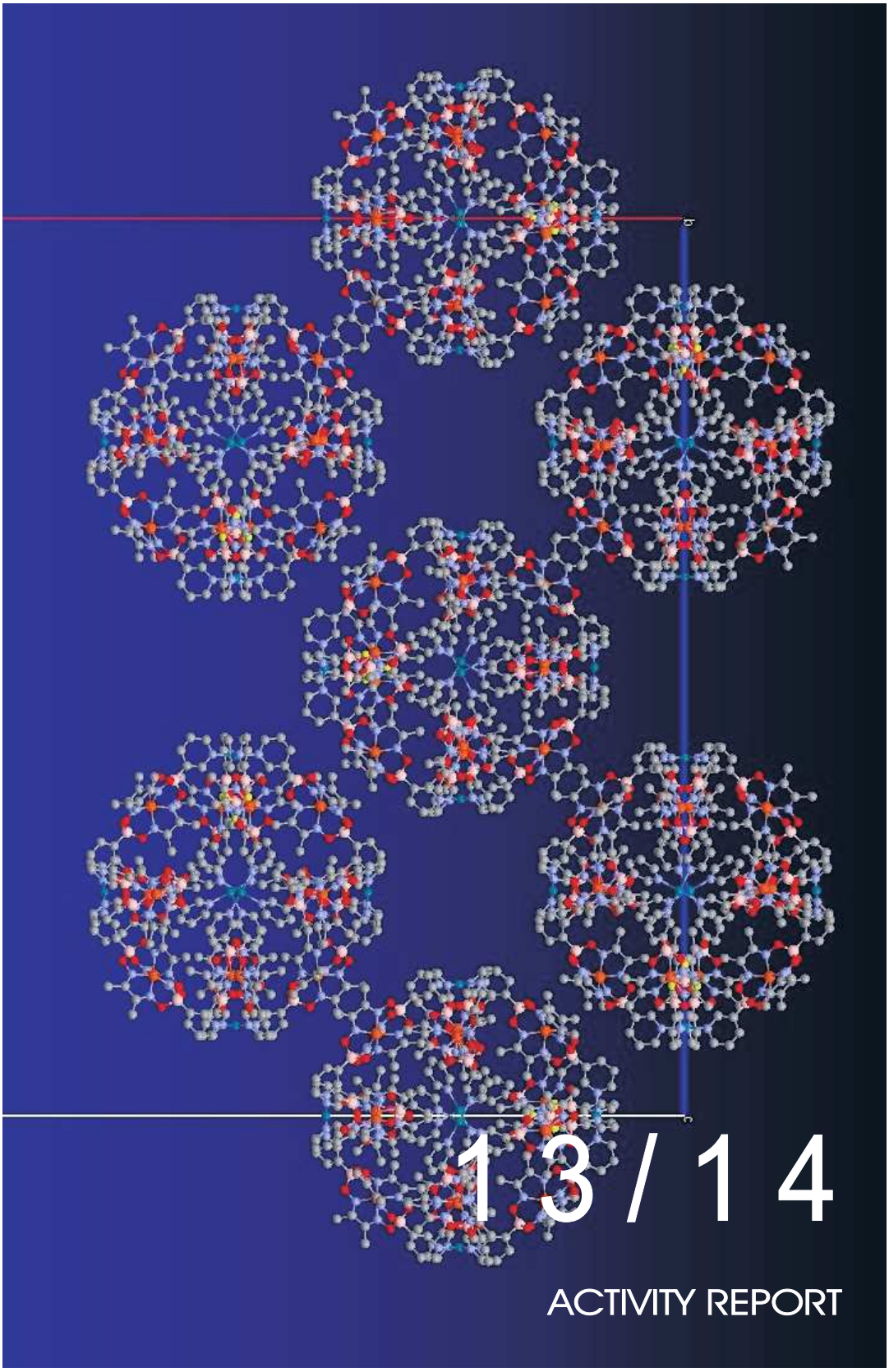

13 / 14

ACTIVITY REPORT

CONTENTS

INTRODUCTION

The Swiss-Norwegian Beamline project has now reached a crossroads. We can look back on almost twenty years of successful operation of BM01, during which well over a 1000 publications have appeared using data from SNBL. In the coming decade, the configuration of the beamlines will change dramatically. The move of BM01B to BM31 has been strongly supported, both by our stakeholders in Norway and Switzerland and by the ESRF management, and the final go-ahead has been given at the end of 2014. By the middle of 2016, the two beamlines which comprise SNBL will begin operation from two separate bending magnet ports. This new configuration will not only provide fresh impetus to the technical and scientific developments taking place on both beamlines, but is absolutely essential if SNBL is to profit fully from the planned Upgrade Program Phase II of the ESRF. From 2020 onwards, the existing bending magnet sources will be replaced by mini-wigglers. Not only will the source quality improve dramatically in terms of spectral flux and emittance, but the narrowing of the horizontal divergence of the synchrotron beam means that the split beamline option will no longer be feasible. Therefore the move to BM31 will guarantee the long-term viability of both Swiss-Norwegian beamlines.

As a consequence of the extended five month shut-down of the storage ring in 2012 as part of the ESRF Upgrade Program Phase I, the output in terms of the number of SNBL publications dropped significantly in 2013. Interestingly, this shortfall was quickly recovered in 2014, when once again over 100 papers per year were published using data from SNBL. The main focus of scientific activity is now strongly oriented towards energy-related research. Instrumentation development targeted at *in-situ* experiments has been an important aspect of the beamline work in recent years, particularly for studying catalytic reactions and hydrogen storage. There is a strong emphasis on energy research in Norway and Switzerland covering the social, economic and technical aspects of a more sustainable energy system. Synchrotron radiation sources have an important role to play in this endeavour, and SNBL is particular well-equipped to support

the activities of scientists from both countries. Indeed, the extra space which becomes available after the new beamline comes on-line in 2016 will greatly extend the range and complexity of the *in-situ* experiments which form a crucial part of the energy research carried out on SNBL.

The Memorandum of Understanding (MoU) with the Dutch-Belgian beamline has continued to provide a fruitful basis for collaboration, both in terms of resources (e.g. sharing equipment and manpower) and in facilitating the exchange of beamtime between the two CRGs. In particular, the access to the very successful small-angle scattering branch line on DUBBLE has been extensively used by the Norwegian groups interested in soft condensed matter and polymer research. In return, Dutch and Belgian groups have been frequent visitors to SNBL. Another MoU has been in existence for several years between SNBL and MaxLab in Sweden. This has led to several exchange visits by staff from both laboratories, most recently by the Director of MAXIV, Dr Christoph Quitmann, who attended a meeting of the SNX Council in 2014. The sharing of expertise between the staff of different beamlines, both within the ESRF and with other facilities, has become an increasingly important part of the activities at SNBL. In this context, it is a pleasure to note that two of the postdocs who have served at SNBL (Vadim Diadkin and Volodymyr Svitlyk) have now become members of the scientific staff of the ESRF. We wish them both much success in their new positions.

In 2014, the SNX Council formed a committee under the Chairmanship of Prof Robert Cernik from the University of Manchester together with representatives from Norway and Switzerland, with the task of formulating medium and long-term scientific goals for SNBL up to and including the two funding periods covering the next decade. The report of this committee has now been submitted to the SNX Council and to the funding agencies for consideration. Our challenge in the coming years will be to turn these goals into reality, and hence provide both countries with the synchrotron facilities which truly match their scientific needs.

V. DMITRIEV, P. PATTISON, H. EMERICH

SCIENTIFIC HIGHLIGHTS

110

PUSHING THE LIMITS: GIANT NEGATIVE COMPRESSIBILITY

When squeezed uniformly, the overwhelming majority of materials shrink in all directions. We have discovered that the crystalline compound zinc dicyanoaurate, $Zn[Au(CN)_2]_2$, actually expands under such hydrostatic pressure in a range of directions, and does so at a rate that is many times greater even than the usual compressibility of conventional ceramics. This negative linear compressibility (NLC) response

ESRF

has potential applications in the development of next-generation actuators, pressure sensors, and even artificial muscles [1].

The intuition that materials should shrink under pressure is grounded (rightly) in the underlying thermodynamics: pressure causes the free energy of a system to increase unfavourably unless there is an accompanying reduction in volume. The particular 'trick' of NLC materials such as $Zn[Au(CN)_2]_2$ is to couple volume reduction to linear expansion in one or more directions. In other words, their structures become longer as they become more dense. The wine-rack and honeycomb topologies are two examples of network geometries that respond to pressure in this way [2]. Indeed, we identified $Zn[Au(CN)_2]_2$ as a NLC candidate because its hexagonal crystal structure is based on the quartz topology, itself a three-dimensional honeycomb network (Figure 134).

Variable-pressure powder X-ray diffraction (PXRD) measurements, carried out using **BM01A**, the Swiss-Norwegian beamline, enabled us to determine how the crystal structure of $Zn[Au(CN)_2]_2$ changes when exposed to pressures of up to 14 GPa. From the variation in lattice parameters, we determined the crystal compressibilities, and by refining structural models against the diffraction intensities we could also monitor the accompanying changes in network geometry.

The compressibilities of conventional ceramics are usually around 5 TPa^{-1}, meaning a decrease in length of 0.5% for each 1 GPa pressure interval. For $Zn[Au(CN)_2]_2$, we measured compressibilities of +52(6) and −42(5) TPa^{-1} along directions perpendicular and parallel to the [001] hexagonal crystal axis. These values become smaller at the very highest pressures (as one expects); nevertheless by the end of our experiment the sample had grown by roughly 10% along the NLC direction (Figure 135). The long-standing 'record' response amongst the dozen or so previously-known NLC materials was just −1.2 TPa^{-1} (for elemental selenium), making the 'giant' NLC effect of $Zn[Au(CN)_2]_2$ all the more remarkable.

Our structural refinements revealed two key features responsible for such large compressibilities in this material. The first is that throughout the entire experiment there is remarkably little change to individual bond lengths and coordination geometries: the open framework structure, assembled from zinc 'nodes' and dicyanoaurate 'linkers' simply flexes in a way that would be expected to carry very little energy cost. The second feature is that the 'shock' of compressing this network so very rapidly in directions perpendicular to the [001] axis is accommodated by atomic-scale 'springs' assembled from highly polarisable gold atoms. So our study shows how a combination of structural engineering and supramolecular chemistry motifs might be coupled in order to design functional materials with counterintuitive mechanical responses.

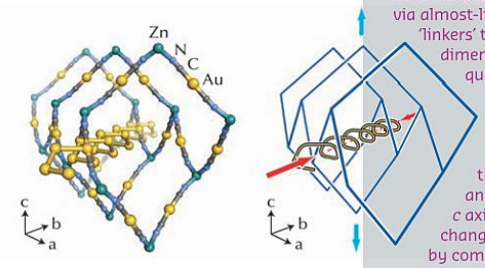

Fig. 134: The crystal structure of $Zn[Au(CN)_2]_2$ is assembled from tetrahedral Zn 'nodes', connected via almost-linear dicyanoaurate 'linkers' to give a three-dimensional network with the quartz topology. Under increasing hydrostatic pressure, this network reduces its volume by compressing along the *a* and *b* directions and expanding along the *c* axis. Rapid geometric changes are accommodated by compression of spring-like chains of gold atoms connected via weak 'aurophilic' interactions.

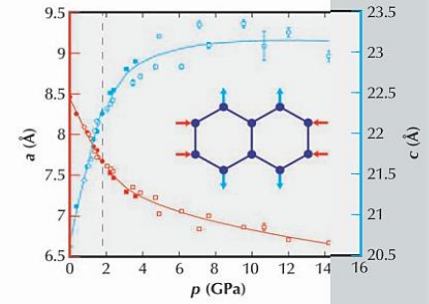

Fig. 135: Pressure-dependent variation in lattice parameters measured using PXRD. The NLC behaviour of $Zn[Au(CN)_2]_2$ is evident in the anomalous increase in the *c* lattice parameter with pressure. The vertical dashed line denotes a displacive phase transition to a related superstructure that also shows NLC.

Principal publication and authors
A.B. Cairns (a), J. Catafesta (b,c), C. Levelut (c) J. Rouquette (b), A. van der Lee (d), L. Peters (e), A.L. Thompson (a), V. Dmitriev (f), J. Haines (b) and A.L. Goodwin (a), *Nature Materials* **12**, 212–216 (2013).
(a) Inorganic Chemistry Laboratory, Department of Chemistry, University of Oxford (UK)
(b) Institut Charles Gerhardt, Université Montpellier 2, Montpellier (France)
(c) Laboratoire Charles Coulomb, Université Montpellier 2, Montpellier (France)
(d) Institut Européen des Membranes, Université Montpellier 2, Montpellier (France)
(e) Institut für Kristallographie, RWTH Aachen, Aachen (Germany)
(f) Swiss-Norwegian beamline, ESRF

References
[1] R. Baughman, S. Stafstrom, C. Cui and S. Dantas, *Science* **279**, 1522-1524 (1998).
[2] J. Grima, D. Attard, R. Caruana-Gauci and R. Gatt, *Scr. Mater.* **65**, 565-568 (2011).

MIXED-LINKER HYBRID SUPERPOLYHEDRA FOR LARGE-PORE IRON(III) CARBOXYLATE METAL–ORGANIC FRAMEWORKS

Principal publications and authors
H. Chevreau (a), T. Devic (a), F. Salles (b), G. Maurin (b), N. Stock (c) and C. Serre (a), *Angew. Chem. Int. Ed.*, **52**, 5056-5060 (2013).
(a) Institut Lavoisier de Versailles, CNRS, Université de Versailles St-Quentin en Yvelines (France)
(b) Institut Gerhardt, CNRS, ENSCM, Université de Montpellier (France).
(c) Institut fur Anorganische Chemie, Christian-Albrechts-Universität, Kiel, (Germany)

Metal organic frameworks (MOFs) are attracting great interest for their potential in various applications ranging from gas capture to storage to catalysis. While most of the solids reported in the literature are based on M^{2+} cations (*e.g.* Zn^{2+}, Cu^{2+}, Ni^{2+}), M^{n+} with n ≥ 3 (Fe^{3+}, Al^{3+}, Cr^{3+}, Zr^{4+}, Ti^{4+}) species have been shown to induce higher chemical stabilities [1], which is often a prerequisite for further industrial applications. Among these cations, Fe^{3+} deserves special attention due to its low toxicity, which makes the resulting solids highly suitable for bio-applications such as drug release [2]. While the structural diversity is mainly induced by building structures with more and more complex organic ligands, an alternative consists of the use of a mixture of simple ligands with different symmetries. Applying such a strategy with linear dicarboxylic and planar tricarboxylic ligands, we were able to generate two series of original Fe^{3+} MOFs built up from hybrid polyhedra. Contrary to the case of the n = 2 counterparts, MOFs based on n ≥ 3 are very often produced in a polycrystalline form, and as a consequence, their structures cannot be solved using laboratory single crystal X-ray diffractometers. Taking advantage of the versatility of the image-plate detector available at **BM01A**, the Swiss-Norwegian beamline, we solved the structures by a combination of single crystal and powder diffraction analyses, assisted with molecular simulations. Using a mixture of 1,4-benzenedicarboxylic acid (H_2-bdc) (**Figure 136b**) and 1,3,5-tris(4-carboxyphenyl)benzene (H_3-btb) (**Figure 136c**), we have generated two solids, both based on the same inorganic unit, which consists of three corner sharing FeO_6 octahedra surrounded by six carboxylate groups (**Figure 136a**). Organic and inorganic units assemble to define hybrid super-polyhedra, built up from Fe trimers at their corner and ligands on their edges (when ditopic) or faces (when tritopic). The structure of the first solid (later called MIL-143, MIL stands for Materials Institut Lavoisier), which was isolated at shorter reaction time, was solved from powder diffraction. Its cubic structure consists of an alternation of two types of hybrid super-tetrahedra, one based on bdc and identical to those found in the single ligand solid MIL-101 [3], and the second one based on btb (**Figure 136**). This defines an extended ß-cristobalite topology and mesoporous cages (**Figure 136**) leading to a high surface area (S_{BET} above 2000 $m^2.g^{-1}$). The structure of the second phase (denoted MIL-142), which was isolated at longer reaction

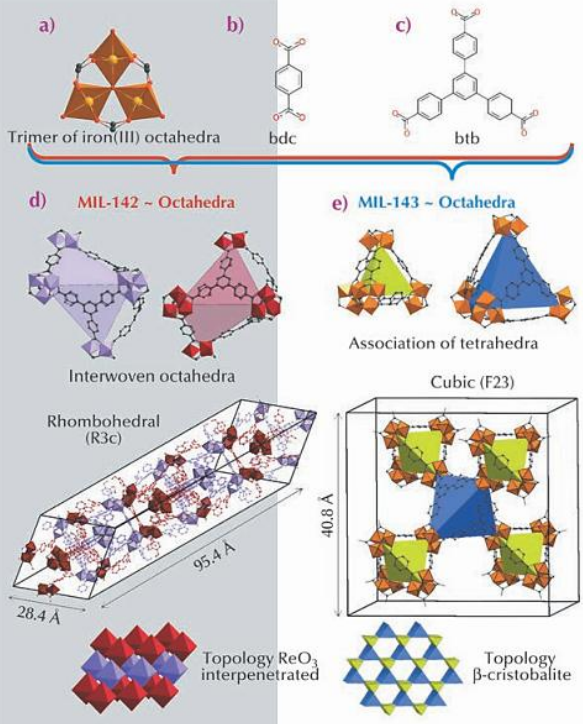

Fig. 136: (a) Trimers of iron(III) octahedra. (b) Terephthalate linker. (c) 1,3,5-tris(4-carboxyphenyl)benzene linker. (d) & (e) Representation and topology of MIL-142 and MIL-143, respectively. Hydrogen has been omitted for clarity.

time, was solved from single crystals. It crystallises in a rhombohedral system with an unusually large *c* parameter (~ 95 Å), and is constructed from a single type of hybrid super-octahedron (SO). The latter is built up from a mixture of ligands, with four faces occupied by btb linkers, and one face defined by three bdc ligands, the remaining faces not being occupied (Figure 136). Such SOs assemble to define a ReO_3 network type, the whole structure being ultimately built from two such interwoven networks, leading to micropores (~ 7-10 Å) and a surface area around 1500 $m^2.g^{-1}$.

In a last step, using longer, functionalised dicarboxylate ligands, the MIL-142 and MIL-143 series were extended through an isoreticular approach. The structure of these solids was determined through a computational assisted approach (experimental unit-cells combined with simulated structures derived from the known ones); analyses included the impact of the functionalisation on the pore size and shape.

References
[1] J.J. Low, A.I. Benin, P. Jakubczak, J.F. Abrahamian, S.A. Faheem and R.R. Willis, *Journal of the American Chemical Society* **131**, 15834-15842 (2009).
[2] P. Horcajada, T. Chalati, C. Serre, B. Gillet, C. Sebrie, T. Baati, J.F. Eubank, D. Heurtaux, P. Clayette, C. Kreuz, J.-S. Chang, Y.K. Hwang, V. Marsaud, P.-N. Bories, L. Cynober, S. Gil, G. Férey, P. Couvreur and R. Gref, *Nat. Mater.* **9**, 172-178 (2010).
[3] G. Férey, C. Mellot-Draznieks, C. Serre, F. Millange, J. Dutour, S. Surblé and I. Margiolaki, *Science* **309**, 2040-2042 (2005).

FROM DISCOVERY TO INVENTION – RATIONAL DESIGN OF ZEOLITES

Since their discovery, zeolites have become the heavy duty molecular machinery of the chemical industry. With their unique porous frameworks, these crystalline aluminosilicates are essential as catalysts and adsorbents for a wide range of applications in petrochemistry, environmental chemistry and water treatment. Despite their importance, the fraction of zeolites used in commercial applications represents less than 10% of all zeolite frameworks hitherto described. This contrast originates from the fact that new zeolites, up to now, have either been discovered in geological deposits or in trial and error syntheses. Until now, rational design of new frameworks to fulfil a specific function in chemical processes has been out of reach. However, the need for reconversion of our fossil fuel based economy makes the availability of zeolites with a tailored framework structure and functionality more important than ever.

Currently, zeolite synthesis exploits mono-, oligo- and polymeric sources of framework elements. The resulting zeolite topologies depend on a large number of parameters and the outcome of most syntheses remains unpredictable. Envisioning rational zeolite design, pre-fabricated building units have been proposed as an alternative to monomeric or colloidal species. Re-assembly of building units existing in a known zeolite provides a promising route. Such building units can for example be harvested by controlled disassembly of existing zeolites. Upon isolation, the building units obtained can be rearranged. Essentially, this comes down to the transformation of existing zeolites into new frameworks with tailored properties.

Recently, two new zeolites COK-14 and –COK-14 were created via this approach. COK-14 is the first material with a new all-silica framework topology (OKO framework) with a two-dimensional channel system and interconnecting 8-, 10- and 12-membered rings (Figure 137). In its interrupted form, called –COK-14, the zeolite additionally has silanol groups pointing systematically into the 12-membered ring (Figure 137). To synthesise these zeolites, building units from the existing IM-12 zeolite were harvested and selectively rearranged. The structure of IM-12 zeolite consists of all-silica sheets interconnected by cubic struts containing one germanate and one silicate four-ring (4R). Acid treatment selectively removes the germanate 4R from the framework leaving the silicate 4R attached to the intact silicate sheets. This structure is consequently recycled as a building

Principal publication and authors
E. Verheyen (a), L. Joos (b), K. Van Havenbergh (c), E. Breynaert (a), N. Kasian (a, d), E. Gobechiya (a), K. Houthoofd (a), C. Martineau (e), M. Hinterstein (f), F. Taulelle (e), V. Van Speybroeck (b), M. Waroquier (b), S. Bals (c), G. Van Tendeloo (c), C. E.A. Kirschhock (a) and J.A. Martens (a), *Nat. Mater.* **11**, 1059-1064 (2012).
(a) Center for Surface Chemistry and Catalysis, KU Leuven, Heverlee (Belgium)
(b) Center for Molecular Modeling, Ghent University, Zwijnaarde (Belgium)
(c) Electron Microscopy for Materials Science, University of Antwerp (Belgium)
(d) L.V. Pisarzhevsky Institute of Physical Chemistry, National Academy of Sciences of Ukraine, Kyiv (Ukraine)
(e) Tectospin, Institut Lavoisier, UMR 8180 Université de Versailles Saint Quentin en Yvelines (France)
(f) Institut für Werkstoffwissenschaft, Technische Universität Dresden (Germany)

unit and reconnected into COK-14 or –COK-14, depending on the hydration state. Overall, the transformation from IM-12 to COK-14 involves the removal of one layer of T-atoms and as such is the first experimentally observed inverse sigma transformation.

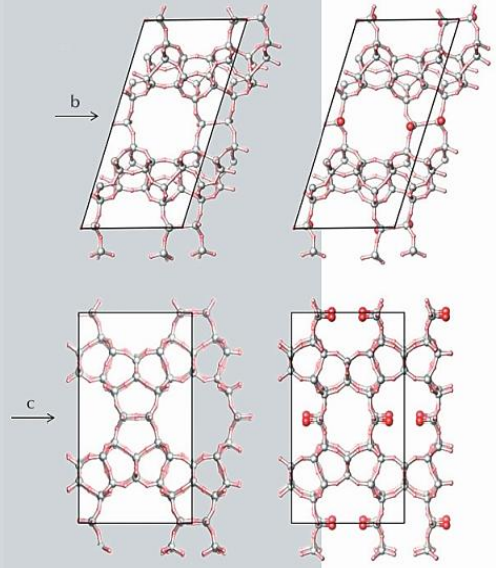

Fig. 137: COK-14 framework (left) and -COK-14 framework (right). OH groups in –COK-14 are highlighted in red.

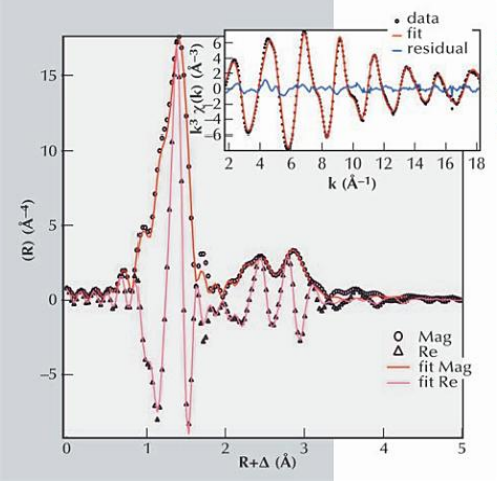

Fig. 138: k_3 weighted Ge K-edge EXAFS data as inset and its Fourier transform (magnitude/ real part) for IM-12.

The choice for IM-12 zeolite as a source of building units resulted from its interesting geometry of silicate layers connected by germanate and silicate four-rings. The arrangement of germanium (Ge) in this zeolite was analysed by Ge K-edge EXAFS at **BM01B**, the Swiss Norwegian Beamline (SNBL), in collaboration with **BM26**, DUBBLE Beamline. EXAFS analysis revealed that each Ge centre was connected to 4 oxygen atoms (3+1) at respectively 1.75 Å and 1.85 Å (**Figure 138**) and two Ge neighbours at 3.16 Å. In combination with high resolution powder X-ray diffraction (HRXRD) data obtained from the same sample, this geometric unit was localised unambiguously as a germanate 4R in the cubic unit connecting all-silicate layers in the structure of IM-12.

Ge K-edge EXAFS and HRXRD measurements were of key importance to reveal the Ge distribution in IM-12. The presence of a Ge four-ring in the structure allowed us to isolate separate silicate building units. These can be alternatively stacked to form new zeolites in a more rational zeolite synthesis approach. Discovering the ordered arrangement of Ge in IM-12 zeolite not only led to the synthesis of new zeolites –COK-14 and COK-14. With this knowledge, we are now studying the synergy between the overall zeolite synthesis conditions and the final Ge arrangement in the framework. This leads to several new synthesis approaches for obtaining similar Ge distributions in a zeolite.

SHORT-RANGE CORRELATIONS IN MAGNETITE ABOVE THE VERWEY TEMPERATURE

Magnetite, Fe_3O_4, is the first magnetic material discovered and utilised by mankind in Ancient Greece, yet it still attracts attention due to its puzzling properties. Discovered in the first half of the twentieth century, the Verwey transition in magnetite [1] remains one of the most intriguing phenomena in solid-state physics. Magnetite is a ferrimagnet with an anomalously high Curie temperature T_C = 850 K. Hence, it is viewed as an ideal candidate for room-temperature spintronic applications. It crystalises in the inverse spinel cubic structure, with two types of Fe sites: the tetrahedral A sites and the octahedral B ones. At T_V = 124 K, a first-order phase transition occurs as the electric conductivity drops by two orders of magnitude with the simultaneous change of the crystal structure from the cubic to monoclinic symmetry and with

Principal publication and authors
A. Bosak (a), D. Chernyshov (b), M. Hoesch (c), P. Piekarz (d), M. Le Tacon (e), M. Krisch (a), A. Kozłowski (f), A.M. Oleś (e,g) and K. Parlinski (g), *Phys. Rev. X* 4, 011040 (2014).
(a) ESRF
(b) SNBL, ESRF
(c) Diamond Light Source, Didcot (UK)
(d) Institute of Nuclear Physics, Polish Academy of Sciences, Kraków (Poland)
(e) Max-Planck-Institut für Festkörperforschung, Stuttgart (Germany)
(f) AGH-University of Science and Technology, Kraków (Poland)
(g) Marian Smoluchowski Institute of Physics, Jagellonian University, Kraków (Poland)

References
[1] E.J.W. Verwey, *Nature* **144**, 327 (1939).
[2] A. Faber, in *Spectroscopy Techniques*, B. Richards, H. Evans (Eds.), Oxford University Press, New York, 1-34 (1999).

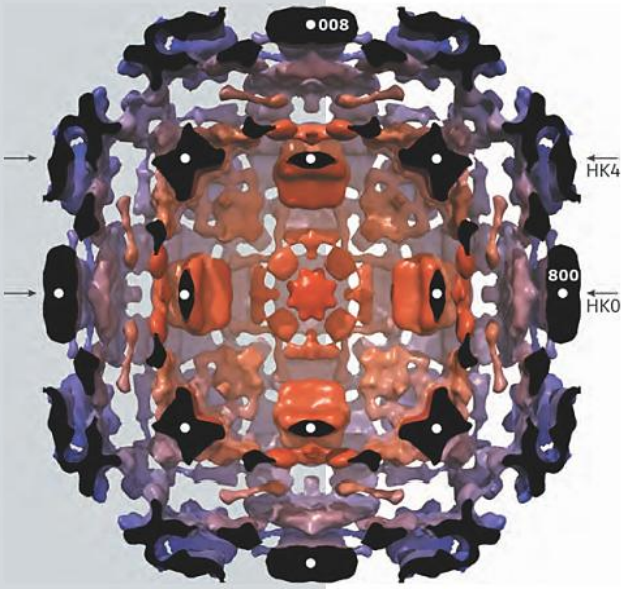

Fig. 146: Isosurface representation of diffuse scattering in magnetite slightly above T_V. Colour represents the distance to the (000) node; diffuse clouds in the proximity of weak Bragg spots have been removed. The half-space above the H0L plane has also been removed. White circles mark strong Bragg reflections in the H0L plane, and arrows denote HK0 and HK4 cuts perpendicular to the image plane.

spectacular anomalies in practically all physical characteristics. The low-temperature structure of magnetite, as deduced from recent studies, was identified to be of monoclinic Cc space group symmetry, with a complex displacement pattern [2]. This suggests that electron localisation, responsible for the dramatically increased resistivity, appears in basic three-Fe-site units, called "trimerons".

With the use of a state-of-the-art large area detector (PILATUS 6M), a detailed three-dimensional (3D) reciprocal space mapping can be performed, revealing an extremely rich diffuse scattering pattern (Figure 146), inherited from the complex low-temperature structure below the Verwey transition. Even at room temperature, which is considerably higher than the 124 K transition temperature, electrons appear to be correlated over relatively large length scales (Figure 147). The characteristic length estimated from the width of diffuse features varies from ~2 unit cells (u.c.) of the prototype cubic structure at T_V+2.5 K to a value slightly larger than ~1 u.c. at room temperature. Thus, the ordering pattern cannot be reduced to the trimeron features, but rather to complexes of trimerons. Therefore, our study supports the polaron picture, and we can state that its structure is in reality much more complex than ever expected previously. We were able to associate some characteristic experimental features with the topology of the Fermi surface of magnetite. While the structure of the low-temperature phase was frequently considered as a key to the understanding of the Verwey transition, our work indicates that the diffuse scattering pattern *above* the transition actually encodes some key information.

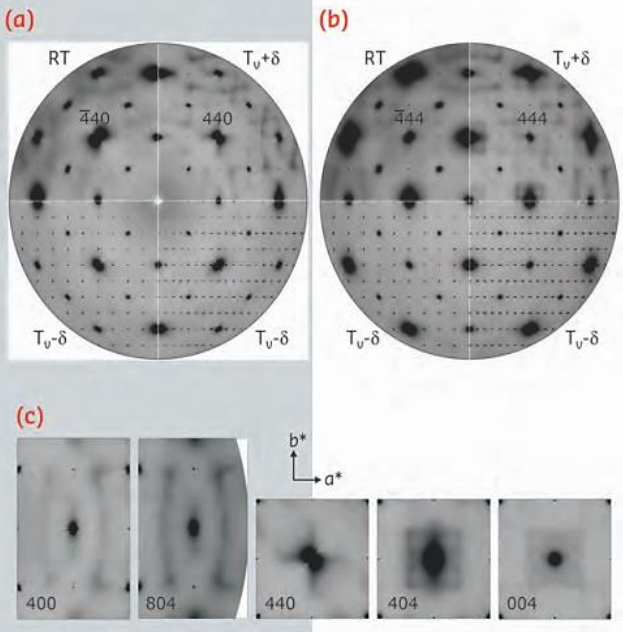

Fig. 147: Diffuse scattering in magnetite at variable temperature. Magnetite reciprocal space cuts HK0 (a) and HK4 (b) are shown at room temperature (RT), slightly above (T_V + δ) and below (T_V − δ) the Verwey transition, with δ ~ 2.5 K. Left-hand bottom panels: Sections perpendicular to the cell doubling direction. Right-hand bottom panels: sections parallel to the cell doubling direction. Selected regions of interest (see text) are shown in (c) together with the unit cell vectors a* and b*. Cubic m3m (above T_V) and tetragonal 4/mmm (below T_V) Laue symmetries have been applied.

PUSHING CRYSTALLOGRAPHY ACROSS THE NUCLEATION BARRIER

Principal publication and authors
C. Tyrsted (a), N. Lock (a), K.M.Ø. Jensen (a,b), M. Christensen (a), E.D. Bøjesen (a), H. Emerich (c), G. Vaughan (d), S.J.L. Billinge (b) and B.B. Iversen (a), IUCr-J 1, 165-171 (2014).
(a) Center for Materials Crystallography, Department of Chemistry, and iNANO, Aarhus University (Denmark)
(b) Department of Applied Physics and Applied Mathematics, Columbia University, New York (USA)
(c) SNBL, ESRF
(d) ESRF

The century-old technique of X-ray diffraction continues to become ever more important for materials characterisation, laying the foundation for many scientific and technological advances in academia and industry alike. The rapid progress in X-ray diffraction methods has made it possible for researchers to routinely identify known materials and solve the structures of previously unknown compounds. The key requirement being that the material exhibits a crystalline long range ordering of the atomic lattice, the prerequisite for Bragg diffraction. Digging into the world of nanoscience, the coherent atomic domains of materials become ever smaller, challenging the condition for Bragg diffraction. This has meant that crystallography was often disregarded in the structural characterisation of amorphous, liquid and extremely nanocrystalline systems. However, this perception is quickly changing, partly owing to the further development and growing use of total scattering experiments and pair distribution function (PDF) analysis [1].

In material science, it is a grand challenge to understand the atomic ordering of materials during synthesis. By knowing the mechanism of crystal formation it may be possible to control it, thereby tailoring desired materials. This is especially a keen interest in the field of solvothermal synthesis [2], where crystalline materials often form from dissolved chemical species or otherwise disordered gel systems. While the evolution of the growing crystalline particles themselves may be followed by diffraction, a barrier is met when trying to understand the local structures existing at the point of nucleation or the stage(s) preceding it.

In this study, total X-ray scattering in combination with X-ray absorption spectroscopy was used in an attempt to further the understanding of the formation of yttria-stabilised zirconia nanoparticles during solvothermal processing. Under these conditions (methanol-based solution at T = 275°C and P = 250 bar), dissolved Zr^{4+} and Y^{3+} species are transformed into crystalline $Zr_{1-x}Y_xO_{2-\delta}$ nanoparticles in a matter of minutes. Visually, the system may be observed to change from a translucent solution to an apparent gel-like structure upon nucleation, steadily densifying with prolonged hydrothermal processing. Therefore, three different structural stages likely exist during different points in this process: 1) pre-nucleation molecular species, 2) a disordered amorphous network and 3) an ordered crystal lattice. The experimental PDF's representing these different structural stages are shown in Figure 142. Only the third structural stage exhibits Bragg diffraction, the first two stages giving rise to diffuse scattering alone, excluding the use of standard Bragg crystallography. Nonetheless, total scattering clearly proves the existence of distinct local atomic structuring in all three stages spanning further than the first immediate coordination shell.

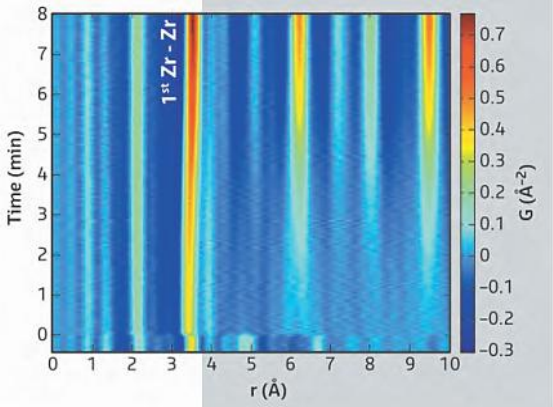

Fig. 142: Local atomic ordering as revealed by total scattering. (d) Time-resolved view of the local structural region (0–10 A°) of the PDF.

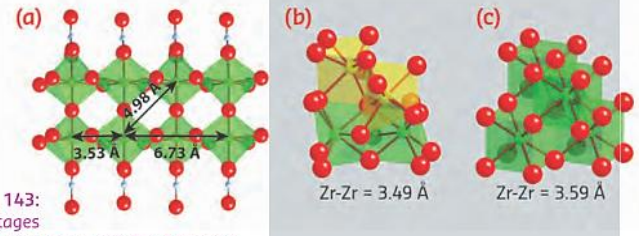

Fig. 143: Structural stages observed during yttria-stabilised zirconia formation. (a) Proposed solution species structure. (b) Amorphous network structure. (c) Mature cubic crystalline structure of YSZ.

SCIENTIFIC HIGHLIGHTS

STRUCTURE OF MATERIALS

The structures found to best describe these structural stages are shown in Figure 143. The local structure found in the pre-nucleation stage is proposed to consist of polymeric zirconia species, formed during dissolution or present in the solid precursor from the beginning. At the point of nucleation, the data indicate that the polymeric species are rapidly fragmented into smaller species which cluster together and precipitate out as an amorphous network. The atomic network of the precipitate is not entirely randomised despite the apparent chaotic nucleation process, but has a local ordering which may be described as monoclinic in nature. The local bonding environment of the precipitate is therefore not too far from the cubic lattice structure of the end product, yet lacks the correct long range topology. Over time, bond reforming ensures that the local domains order within themselves and in relation to each other thereby forming the desired cubic lattice structure.

Numerous simplified models exist to describe crystal nucleation and growth phenomena. The present study provides the first experimental atomistic insight into the very complex chemical processes that take place during crystallisation, and the total scattering technique provides a new approach to truly understanding nanomaterial formation.

References
[1] T. Egami and S.J.L. Billinge. *Underneath the Bragg peaks: structural analysis of complex materials*. Vol. 16. Newnes (2012).
[2] K.M. Jensen, C. Tyrsted, M. Bremholm and B.B. Iversen, *ChemSusChem* **7**, 1594-1611 (2014).

Crystal chemistry and thermal properties of rare-earth (RE) borohydrides

C. Frommen[1], J. E. Olsen[1], M. D. Riktor[1,2],A. O. Kydland Lysdal[1,3], M. Heere[1], M. H. Sørby[1]and B. C. Hauback[1]

[1]*Physics Department, Institute for Energy Technology, P. O. Box 40, NO-2027, Kjeller*
[2]*SINTEF Materials and Chemistry, Forskningsveien 1, NO-0314, Oslo*
[3]*Department of Physics, Norwegian University of Science and Technology, NO-7491, Trondheim*

Solvated rare-earth (RE) borohydrides and their complexes are widely used in organometallic chemistry as selective reducing agents and Ziegler-Natta catalysts for the polymerization of certain dienes [1] or the ring-opening polymerization of cyclic esters [2]. Solvent free RE borohydrides on the other hand have only recently become available [3]. They have received considerable attention during the past 5 years due to their rich crystal chemistry [4-11] and potential as both solid state hydrogen storage materials [12-14] and solid state electrolytes [15-17]. The standard technique for the synthesis of RE borohydrides is via mechanochemical reaction between a RE chloride and a light-weight metal borohydride (mostly $LiBH_4$). Our group has performed a systematic study on the formation of RE borohydrides and we have recently reviewed the crystal chemistry and thermal properties of ball-milled mixtures between $RECl_3$ and $LiBH_4$ [4, 5]. The following sections present highlights of our experimental synchrotron radiation powder X-ray diffraction (SR-PXD) work performed on stations BM01A and BM01B of the Swiss-Norwegian beamlines, SNBL.

Structure types: RE-borohydrides form four distinct structure types which are determined by the ionic radius of the RE element and its electronic configuration. The early lanthanides (La, Ce, Pr and Nd) with the largest ionic radius form $LiRE(BH_4)_3Cl$ compounds (cubic; *I*-43*m*) [5]. $LiCe(BH_4)_3Cl$ is the first-anion-substituted and mixed-metal RE-borohydride reported in the literature and its unit cell contains octahedrally coordinated Ce atoms (3×BH_4, 3×Cl) [7]. A unique structural feature of this compound is a distorted Ce_4-Cl_4 hetero-cube (Figure 1). There remains some speculation about the location of the Li atom in the unit cell. One model describes the structure with two lithium atoms: one in the (6b) position at (0 ½ ½) and the second in (2a) at (0 0 0) [7]. An alternative model describes the Li atoms as being disordered, occupying 2/3 of the (12d) Wyckoff site [16]. The very high Li-ion conductivity of 10^{-4} S/cm at 20 ^{o}C seems to be in accordance with the disorder in Li positions [16].

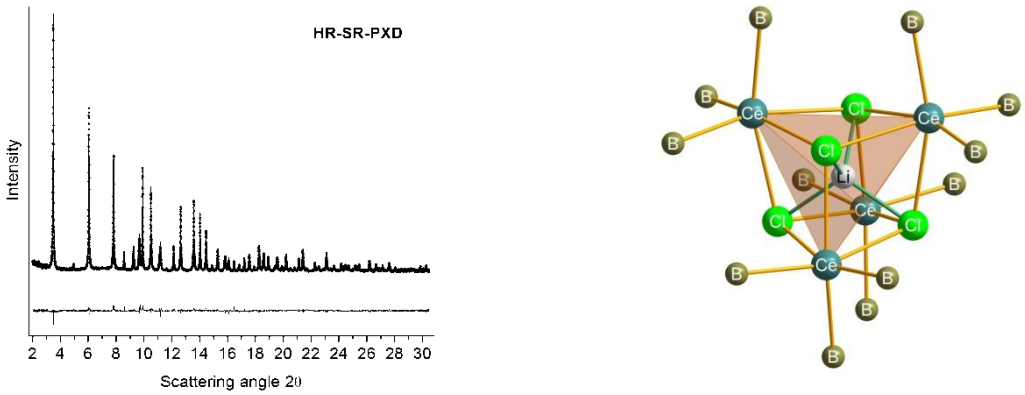

Figure 1: High-resolution (HR) SR-PXD pattern (λ = 0.50123 Å) and core-structure of $LiCe(BH_4)_3Cl$ with a possible Li-position in the centre of the Ce_4-Cl_4 hetero-cube [7].

The elements in the middle and towards the end of the series (Sm, Gd, Tb, Er and Yb) yield α-$RE(BH_4)_3$ compounds (cubic; *Pa*-3) with a possible polymorphic transition to β-$RE(BH_4)_3$ for Sm, Er and Yb (cubic; *Pm*-3*m* or *Fm*-3*c*) [4]. These compounds are isostructural to α-$Y(BH_4)_3$ and β-$Y(BH_4)_3$, respectively [6]. Their unit cell is related to the ReO_3-structure in which the metal atoms form a metal-cube and BH_4 groups are oriented along the cube edges, leading to an octahedral coordination around each metal atom (Figure 2). The α-polymorph can be considered a distorted variant of the ReO_3 structure type whereas the β-polymorph represents the regular ReO_3 structure type. Sm and Gd also exhibit transitions to the $LiRE(BH_4)_3Cl$ structure type that is observed for the largest lanthanide ions.

Figure 2: Unit cell for two different $RE(BH_4)_3$ polymorphs: α-$RE(BH_4)_3$ (left) and β-$RE(BH_4)_3$ (right) as seen by SR-PXD, with RE atoms shown as light grey spheres. Note the disordered structure [18] (*Pm*-3*m*, a~5.5Å) on the right which becomes ordered (*Fm*-3*c*, a~11Å) when neutron diffraction is used instead [6].

The smallest lanthanides Yb and Lu form tetrahedral $[RE(BH_4)_4]^-$ anionic complexes that are stablilized by Li^+ cations (tetragonal; *P*-42*c*) in analogy to the structure of $LiSc(BH_4)_4$ [4, 19]. Rietveld refinement for the Yb-containing borohydride phase showed that this compound is in fact chloride substituted and must be described as $LiYb(BH_4)_{4-x}Cl_x$ (x=1.0). A particularly rich crystal-chemistry is observed in the $YbCl_3$-$LiBH_4$ system, where numerous compounds are formed depending on experimental conditions, e.g. molar ratio of the starting materials, milling time or heat treatment [5]. Ball-milling may lead to three different Yb-containing borohydride phases: (1,2) α/β-$Yb(BH_4)_3$, with six-coordinated and trivalent Yb and $[BH_4]$ groups shared between 2 Yb atoms; (3) $LiYb(BH_4)_3Cl$ with a four-coordinated and trivalent Yb that contains isolated $[YbX_4]^-$ anions charge-balanced by Li^+ cations. This behaviour can be rationalized in terms of its ionic radius (Yb^{3+}: 0.86 Å) which lies in between those of Y^{3+} (0.90 Å) and Sc^{3+} (0.76 Å). Slight modifications in experimental conditions can therefore result in two different compounds which are isostructural to α/β-$Y(BH_4)_3$ [3, 6, 18] and $LiSc(BH_4)_4$ [19], respectively.

Additionally, two divalent Yb-containing borohydride phases have been obtained during heat treatment. The first one, *tet*-$Yb(BH_4)_{2-x}Cl_x$ (x=0.76), crystallizes in the tetragonal space group *P*-4. The unit cell contains columns of edge-sharing YbX_6 octahedra along the *c*-axis which are furthermore connected by corner-sharing in the *ab*-plane; each BD_4/Cl unit is hereby shared among three YbX_6 octahedra (Figure 3 left). *Tet*-$Yb(BH_4)_{2-x}Cl_x$ is shown to be isostructural to β-$Ca(BH_4)_2$. The second one, *ortho*-$Yb(BH_4)_{2-x}Cl_x$ (x=0.365), crystallizes in the orthorhombic space group *Pbca* and shows a distorted octahedral environment around Yb^{2+} and each BD_4/Cl group is shared among 3 octahedra (Figure 3a).

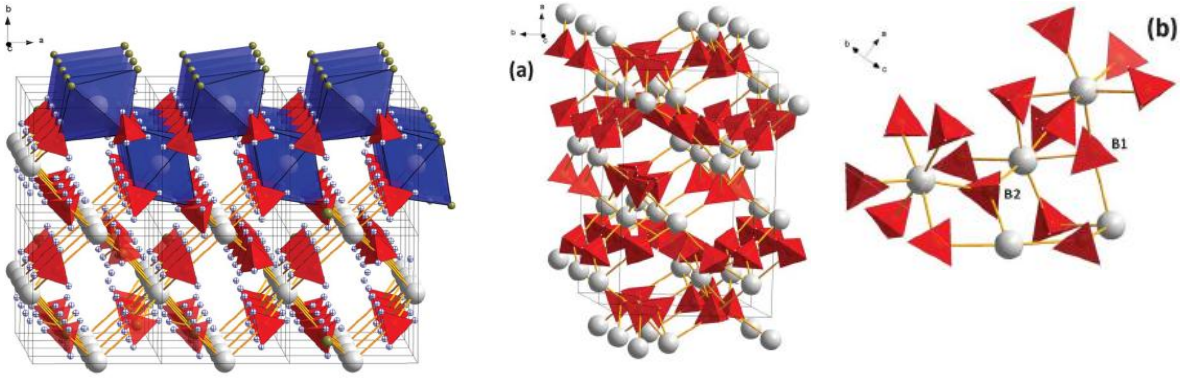

tet-$Yb(BH_4)_{1.24}Cl_{0.76}$ *ortho*-$Yb(BH_4)_{1.635}Cl_{0.365}$

Figure 3: (left) A representative view of a (3×2×4) supercell of *tet*-$Yb(BH_4)_{1.24}Cl_{0.76}$ with Yb atoms as grey balls. The YbX_6 octahedra (X = Cl, BD_4) are represented with blue transparent faces. Cl atoms are not shown as they coincide with B atoms. (a) Structure of *ortho*-$Yb(BH_4)_{1.635}Cl_{0.365}$ with 2 unit cells in the *c*-direction. (b) Coordination around the two different B positions. Yb atoms are shown as grey balls and BH_4 tetrahedra are shown with red semi-transparent phases [5].

There exist 2 B atoms per unit cell, which adopt different coordination schemes: B1 has a T-shaped and B2 a trigonal planar coordination (Figure 3b).
Ortho-$Yb(BH_4)_{2-x}Cl_x$ (x = 0.365) is isostructural to γ-$Ca(BH_4)_2$ and the structural similarities can again be rationalized in terms of the almost identical ionic radii for Yb^{2+} and Ca^{2+}.The $LiBH_4$-$YbCl_3$ system represents the first case where a metal has been reported with different oxidation states in different borohydride phases. For Yb two major factors are responsible for this diversity: its special electronic configuration (Yb^{3+}:$4f^{13}$; Yb^{2+}:$4f^{14}$) and its ionic radii (Yb^{3+}: 0.868 Å; Yb^{2+}: 1.02 Å).
Table 1 summarizes the different structure types that have been obtained by mechanochemical synthesis between $RECl_3$ and $LiBH_4$ for the RE borohydrides.

Table 1: Possible structure types adopted by RE-borohydrides obtained from $LiBH_4$-$RECl_3$ mixtures [4, 5].

	La	Ce	Pr	Nd	Pm	Sm	Eu	Gd	Tb	Dy	Ho	Er	Tm	Yb	Lu
$LiRE(BH_4)_3Cl$	👍	👍	👍	👍		👍		👍							
α-$RE(BH_4)_3$						👍		👍	👍	👍		👍	👍	👍	
β-$RE(BH_4)_3$						👍						👍		👍	
$LiRE(BH_4)_4$														👍	👍
$RE(BH_4)_2$						👍								👍	

Thermal Decomposition: We have followed the thermal decomposition of numerous composite mixtures between $RECl_3$ (RE = La, Ce, Pr, Nd, Sm, Eu, Gd, Tb, Er and Yb) and $LiBH_4$ in a molar ratio of (1:6) by *in/ex-situ* SR-PXD [4]. In addition, the influence of LiH on the rehydrogenation capacity for La/Er/Yb-containing $6LiBH_4$-$RECl_3$-3LiH composites has been investigated [20]. Summing those experiments up, it has become apparent that the composites show a complex behaviour upon heating. Their decomposition proceeds via several steps, sometimes accompanied by the formation of crystalline intermediates but more often alongside the formation of amorphous or nanocrystalline compounds. A unique feature of those composites is a significantly reduced hydrogen release temperature for $LiBH_4$ (200-300 ^oC) as

compared to bulk $LiBH_4$ (>400 ^oC) [21]. SR-PXD data has shown that this drastic reduction is associated with the presence of REH_{2+x} compounds which are the major decomposition products for temperatures below 300 ^oC. These RE-hydrides react with excess $LiBH_4$ and lead to the formation of LiH and RE-borides (REB_4 and REB_6) as the final decomposition products around and above 400 ^oC. As an example, Figure 4 shows *in-situ* SR-PXD data acquired during heating of a $6LiBH_4$–$ErCl_3$ composite mixture under vacuum with characteristic temperature regions marked by horizontal lines.

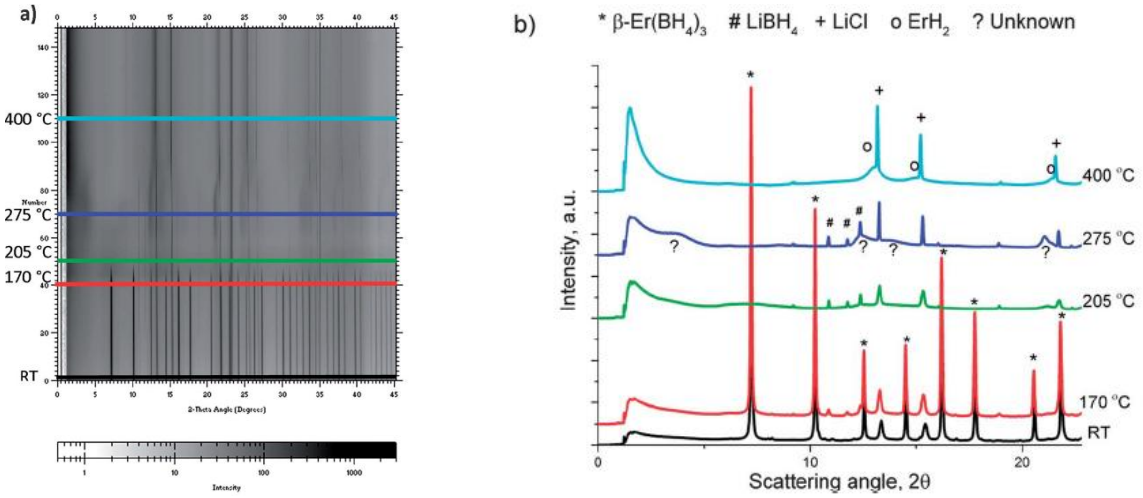

Figure 4: (a) Contour plot of *in-situ* SR-PXD measurements (Pilatus2M, λ=0.69411Å) for a $6LiBH_4$-$ErCl_3$ composite heated under dynamic vacuum (rate: 5^{o}C/min). (b) Diffraction patterns at selected temperatures [4].

The thermal decomposition and rehydrogenation of several composites that contained additional LiH was also followed by *in/ex-situ* SR-PXD [20]. One representative example is shown in Figure 5, which displays SR-PXD patterns at room temperature of a $6LiBH_4$-$ErCl_3$-3LiH mixture after ball-milling, desorption (400 ^oC, 0.5 MPa) and rehydrogenation (340 ^oC, 10 MPa), respectively.

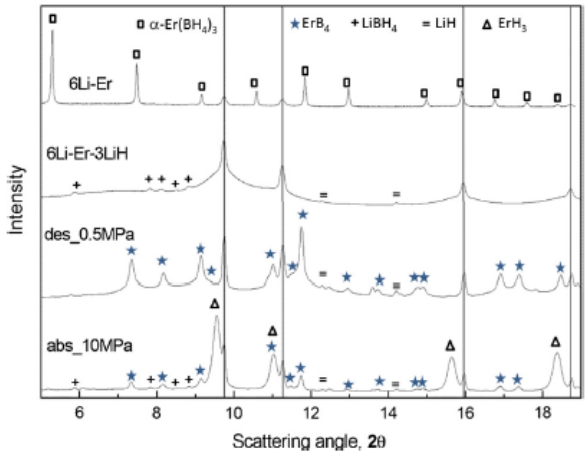

Figure 5: SR-PXD pattern (BM01B, λ=0.50513 Å) of a $6LiBH_4$-$ErCl_3$ mixture after ball-milling (Top), and $6LiBH_4$-$ErCl_3$-3LiH after ball-milling, desorption (0.5 MPa) and rehydrogenation (340^{o}C, 10MPa) [20].

The major crystalline phases after ball-milling are LiCl (vertical line), $LiBH_4$ and LiH. In addition, broad shoulders on either side of the LiCl peaks indicate the presence of additional nanocrystalline compounds, possibly ErH_2 and ErH_3. After thermal decomposition the only crystalline products are ErB_4, LiCl (vertical line) and LiH.

Rehydrogenation of the composite mixture (340^{o}C, 10 MPa) leads to the formation of ErH_3, and the reappearance of $LiBH_4$ at drastically reduced conditions as compared to pure $LiBH_4$ (>400^{o}C, >10MPa). The hydrogen release for this composite mixture reaches about 4.0 wt.% up to 400 ^{o}C, and the rehydrogenation capacity is about 66% when the desorption-rehydrogenation cycle is performed under vacuum/10MPa. This value increases up to 80% when experiments are performed under 0.5/10MPa backpressure [20].

Acknowledgment: The Research Council of Norway is acknowledged for financial support through the FRIENERGI project and the SYNKNØYT program. We furthermore acknowledge the skillful assistance from the staff of SNBL at ESRF.

References:

[1] J. Jenter, N. Meyer, P.W. Roesky, S.K.H. Thiele, G. Eickerling, W. Scherer, Chemistry-a European Journal, 16 (2010) 5472-5480.
[2] M. Schmid, S.M. Guillaume, P.W. Roesky, Organometallics, 33 (2014) 5392-5401.
[3] T. Sato, K. Miwa, Y. Nakamori, K. Ohoyama, H.W. Li, T. Noritake, M. Aoki, S.I. Towata, S.I. Orimo, Physical Review B, 77 (2008).
[4] J.E. Olsen, C. Frommen, T.R. Jensen, M.D. Riktor, M.H. Sørby, B.C. Hauback, Rsc Advances, 4 (2014) 1570-1582.
[5] J.E. Olsen, C. Frommen, M.H. Sørby, B.C. Hauback, Rsc Advances, 3 (2013) 10764-10774.
[6] C. Frommen, N. Aliouane, S. Deledda, J.E. Fonneløp, H. Grove, K. Lieutenant, I. Llamas-Jansa, S. Sartori, M.H. Sørby, B.C. Hauback, Journal of Alloys and Compounds, 496 (2010) 710-716.
[7] C. Frommen, M.H. Sørby, P. Ravindran, P. Vajeeston, H. Fjellvåg, B.C. Hauback, Journal of Physical Chemistry C, 115 (2011) 23591-23602.
[8] T. Jaron, W. Grochala, Dalton Transactions, 39 (2010) 160-166.
[9] W. Wegner, T. Jaron, W. Grochala, International Journal of Hydrogen Energy, 39 (2014) 20024-20030.
[10] W. Wegner, T. Jaron, W. Grochala, Acta Crystallographica Section C-Crystal Structure Communications, 69 (2013) 1289-+.
[11] D.B. Ravnsbaek, L.H. Sorensen, Y. Filinchuk, F. Besenbacher, T.R. Jensen, Angewandte Chemie-International Edition, 51 (2012) 3582-3586.
[12] M.B. Ley, L.H. Jepsen, Y.S. Lee, Y.W. Cho, J.M.B. von Colbe, M. Dornheim, M. Rokni, J.O. Jensen, M. Sloth, Y. Filinchuk, J.E. Jorgensen, F. Besenbacher, T.R. Jensen, Materials Today, 17 (2014) 122-128.
[13] F.C. Gennari, Journal of Alloys and Compounds, 581 (2013) 192-195.
[14] F.C. Gennari, M.R. Esquivel, Journal of Alloys and Compounds, 485 (2009) L47-L51.
[15] M.B. Ley, S. Boulineau, R. Janot, Y. Filinchuk, T.R. Jensen, Journal of Physical Chemistry C, 116 (2012) 21267-21276.
[16] M.B. Ley, D.B. Ravnsbaæk, Y. Filinchuk, Y.S. Lee, R. Janot, Y.W. Cho, J. Skibsted, T.R. Jensen, Chemistry of Materials, 24 (2012) 1654-1663.
[17] A.V. Skripov, A.V. Soloninin, M.B. Ley, T.R. Jensen, Y. Filinchuk, Journal of Physical Chemistry C, 117 (2013) 14965-14972.
[18] D.B. Ravnsbæk, Y. Filinchuk, R. Cerny, M.B. Ley, D. Haase, H.J. Jakobsen, J. Skibsted, T.R. Jensen, Inorganic Chemistry, 49 (2010) 3801-3809.
[19] H. Hagemann, M. Longhini, J.W. Kaminski, T.A. Wesolowski, R. Cerny, N. Penin, M.H. Sørby, B.C. Hauback, G. Severa, C.M. Jensen, Journal of Physical Chemistry A, 112 (2008) 7551-7555.
[20] C. Frommen, M. Heere, M.D. Riktor, M.H. Sørby, B.C. Hauback, Journal of Alloys and Compounds http://dx.doi.org/10.1016/j.jallcom.2015.01.113 (2015).
[21] P. Mauron, F. Buchter, O. Friedrichs, A. Remhof, M. Bielmann, C.N. Zwicky, A. Zuttel, Journal of Physical Chemistry B, 112 (2008) 906-910.

The characterization of molecular nanostructures using synchrotron radiation

Matthew D. Wise,[a] Julian J. Holstein,[b,f] Philip Pattison,[c,d] Celine Besnard,[e] Euro Solari,[a] Rosario Scopelliti,[a] Gerard Bricogne[f] and Kay Severin[a]

[a]*Institut des Sciences et Ingenierie Chimiques, Ecole Polytechnique Federale de Lausanne (EPFL), 1015 Lausanne, Switzerland*
[b]*GZG, Abteilung Kristallographie, Georg-August-Universität Göttingen, Goldschmidtstr. 1, 37077 Göttingen, Germany*
[c]*Swiss-Norwegian Beamline, ESRF, F-38043 Grenoble, France*
[d]*Laboratory of Crystallography, Ecole Polytechnique Federale de Lausanne (EPFL), 1015 Lausanne, Switzerland*
[e]*Laboratory of X-ray Crystallography, University of Geneva, CH-1211-Geneva 4, Switzerland*
[f]*Global Phasing Ltd., Sheraton House, Castle Park Cambridge CB3 0AX, England*

The utilization of transition metal-based self-assembly processes allow the bottom-up preparation of molecular nanostructures. The size and the complexity of the structures which are nowadays accessible is quite remarkable: molecularly defined assemblies with a diameter of 3-5 nm are reported with increasing frequency in the literature, and nanostructures with interesting functions (e.g. specific molecular recognition, catalysis) have become realistic synthetic targets. The Severin group at the EPFL is at the forefront of these developments. Over the last years, the group has developed novel methodologies for the synthesis of very large molecular assemblies. One approach pioneered by the Severin group is based on the simultaneous utilization of two (or more) types of reversible interactions, which are largely orthogonal to one another. Furthermore, a modular approach to prepare long and rigid metalloligands has been developed. These ligands have been used to prepare molecular and polymeric nanostructures. For example, the Severin group has recently published the synthesis and the characterization of palladium-iron-based cage structures which are able to act as hosts for large lipophilic anions (Fig. 1, left). Unpublished results from the Severin laboratory show that some of the newly developed metallo-ligands are ideal building blocks for the construction of metal organic frameworks with very large pores (e.g. Fig.1, right).

For the research projects outlined above, it is of fundamental importance to obtain structural information by single crystal diffraction. Although a modern lab diffractometer is quite capable of producing high quality data for small molecules, the limitations of laboratory data for very large molecules can rapidly become a serious handicap. In recent years, the Severin group at EPFL has developed novel methodologies for the synthesis very large molecular assemblies. This procedure has enabled us to construct large cage molecules with a diameter of more than 3 nm. In a recent example measured at SNBL, the cubic unit cell size was 77.2Å giving a unit cell volume of 459,000 $Å^3$. In total, data on more than 20 different supramolecular compounds have already been collected at SNBL during several beamtime allocations.

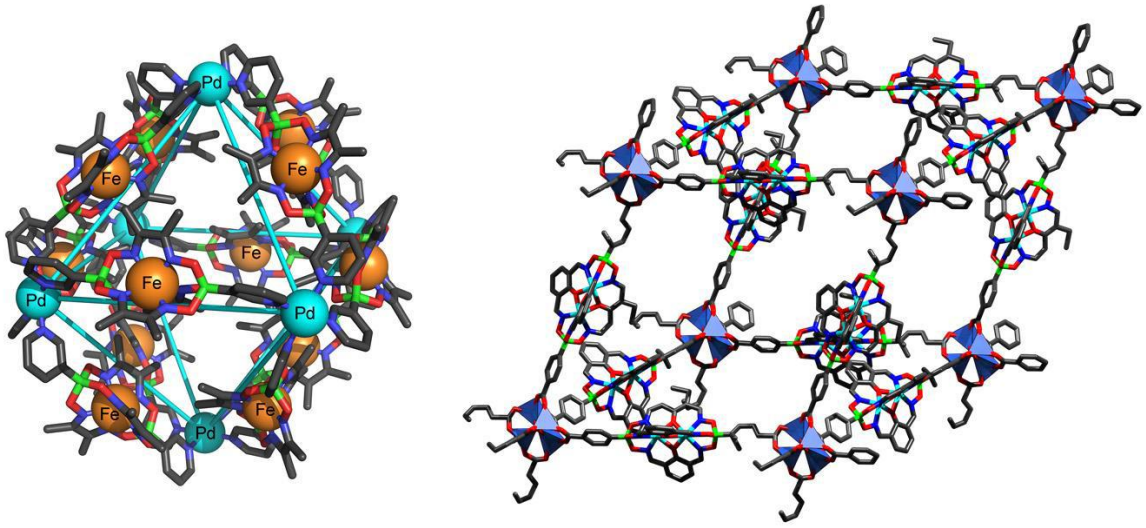

Figure 1. Examples of molecularly defined (left) and polymeric (right) nanostructures prepared in the Severin group.

In Fig 2(a), we present a new structure which has been collected at SNBL at atomic resolution (0.84Å). Final statistics are very good for the size of the structure. In contrast, a similar structure has been measured in-house at the EPFL and the crystals diffract only to 1.4Å resolution. Due to the low number of reflections, it is impossible to refine any of the 1501 independent atoms independently or to model any disorder. This illustrates the importance of access to synchrotron radiation in order to solve structures of this complexity at atomic resolution.
Assemblies of this size pose a number of difficulties due in part to their extensive inherent disorder and high solvent content within the crystal. Synchrotron radiation mitigates some of these difficulties, but we have also employed a series of carefully

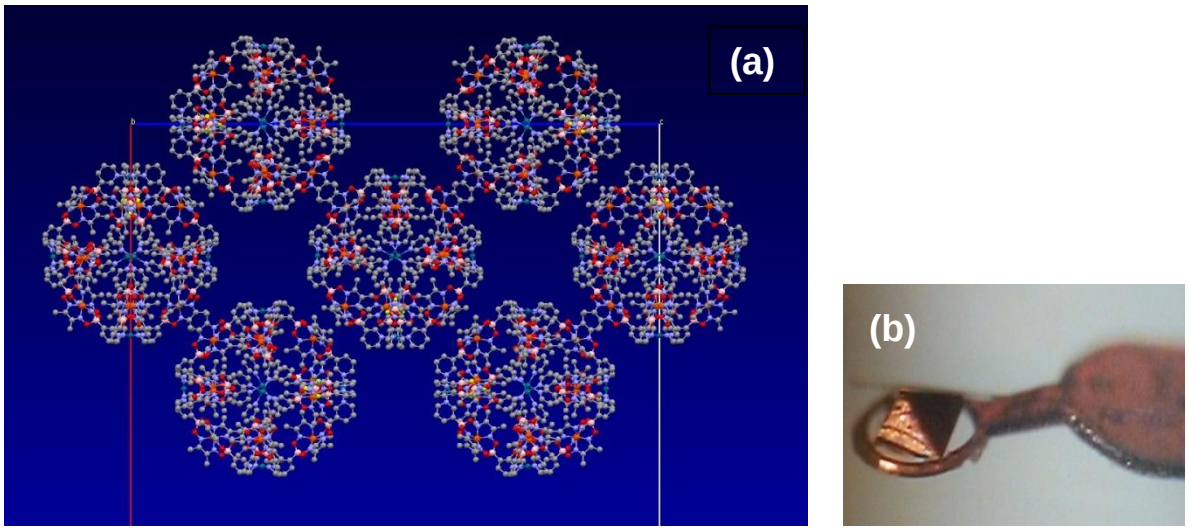

Figure 2. (a) Part of the unit cell of the palladium-iron-based cage structure measured at SNBL/BM01A and **(b)** shows an image of the crystal mounted in a 200 micron loop.

and rigorously adapted macromolecular refinement techniques in order to build a molecular model. These refinement tools have been developed in collaboration with Global Phasing Ltd., Cambridge.

Main publication

Wise, M.D., Holstein, J.J., Pattison, Ph., Besnard, C., Solari, E., Scopelliti, R., Bricognef, G., Severin, K. *Chemical Science***, 6**, 1004-1010 (2015)

Structure and properties of complex hydride perovskite materials

Pascal Schouwink[a],* Morten B. Ley[b], Antoine Tissot[c], Hans Hagemann[c], Torben R. Jensen[b], Ľubomír Smrčok[d] & Radovan Černý[a]

[a]*Laboratory of Crystallography, Department of Quantum Matter Physics, University of Geneva, Quai Ernest-Ansermet 24, CH-1211 Geneva, Switzerland*
[b] *Interdisciplinary Nanoscience Center (iNANO), Department of Chemistry, University of Aarhus, 8000 Aarhus, Denmark*
[c]*Department of Physical Chemistry, University of Geneva, Quai Ernest-Ansermet 30, CH-1211 Geneva, Switzerland*
[d]*Institute of Inorganic Chemistry, Department of Theoretical Chemistry, Slovak Academy of Sciences, Dúbravská cesta 9, SK-845 36 Bratislava, Slovak Republic*

Perovskite-type (Pv) materials are of great technological importance in most fields of materials science, owed to their distinct adjustability of physical properties and the readiness of this very simple octahedral framework to incorporate virtually any chemical element from the periodic table (with exception of noble gases). A slight variation of intrinsic or extrinsic parameters can result in huge changes of physical properties, while the changes to the crystal structure, expressed by lattice distortion and atomic displacements, tend to be hardly noticeable, but of great importance. Metal borohydrides are used in every chemistry laboratory. From being the subject of "highly classified" research during the Manhattan Project they have come a long way, via becoming the most important reducing agents in organic chemistry to contending for solid state hydrogen storage [1].

Chemically, the hydridic nature of the hydrogen in the BH_4-molecule makes borohydrides somewhat an outsider, the covalently bound hydrogen encountered in molecular chemistry commonly carrying a positive formal charge (protic hydrogen). The extreme renewed interest in metal borohydrides during the first years of the millennium was driven by the potential to develop in particular $LiBH_4$ as a solid state hydrogen storage material for on-board automobile applications, hydrogen having the highest mass energy density of any fuel, 120 MJ/kg. The motivation behind metal borohydrides in the materials science community hence directly targeted one of the prime problems of modern consumer societies.

Despite the search for new complex hydrides inevitably being strongly application-oriented, the most important unit, the underling structural architecture of the crystal lattice, is often not being sufficiently considered.

As a consequence, and since metal borohydrides do display significant structural flexibility, which ranges from permanent nano-porous gas hosts to close packed salts, the rational design of borohydride materials is still far from being systematic. Phase diagrams comprise many different polymorphs separated by very small energy barriers, even between compounds of different chemical compositions, largely owed to iono-covalent bonding and vivid structural dynamics. Furthermore, the stability of different phases is sensitive to the synthesis method. Needless to say, such thermodynamic behaviour prevents the theoretical prediction of novel compounds.

A purposeful crystal design is best carried out on a host material of reduced complexity and superior stability. The principal objective of this study was to provide an extensive characterization of a borohydride host materials capable of meeting the requirements of genuine rational and functional design, in order to take metal

borohydrides beyond hydrogen storage applications. Motivated by the first report of a mixed-metal borohydride $KMn(BH_4)_3$ crystallizing with the Pv type [2], this structure type was systematically explored, leading to the discovery of over 45 different materials up to date and allowing us to establish formability criteria for the compound family, based on the Goldschmidt tolerance factor (Figure 1).

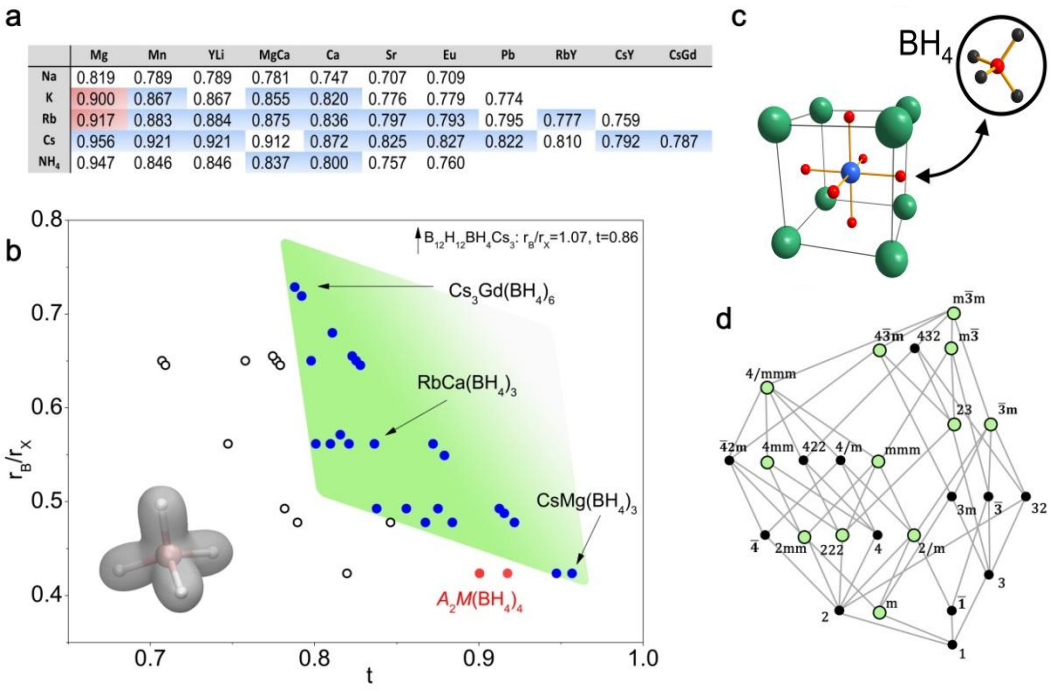

	Mg	Mn	YLi	MgCa	Ca	Sr	Eu	Pb	RbY	CsY	CsGd
Na	0.819	0.789	0.789	0.781	0.747	0.707	0.709				
K	0.900	0.867	0.867	0.855	0.820	0.776	0.779	0.774			
Rb	0.917	0.883	0.884	0.875	0.836	0.797	0.793	0.795	0.777	0.759	
Cs	0.956	0.921	0.921	0.912	0.872	0.825	0.827	0.822	0.810	0.792	0.787
NH_4	0.947	0.846	0.846	0.837	0.800	0.757	0.760				

Figure 1. The established formability field of metal borohydride perovskites shown in green (b) on the basis of octahedral factor vs. tolerance factor *t* (listed in table a). The $AB(BH_4)_3$ structure is shown in (c), highlighting the bidentate coordination mode in an ordered polymorph. (d) Sub-groups derived from the cubic aristotype, e.g. $SrTiO_3$ (STO), green circles correspond to herein reported symmetries.

We began to study this field on ball-milled powder samples using the Dectris PilatusM2 detector at SNBL to systematically ramp the sample in temperature to its decomposition (detection of thermal stability), but also to cycle it over polymorphic transformations in order to investigate the symmetry of lattice instabilities involved in the generation of unusual large superstructures, sometimes appearing as very weak superstructure reflections (hydrogen being a very weak X-ray scatterer).

With the resulting complex hydride materials, we have managed to introduce into metal borohydrides very different and hitherto not at all considered physical properties such as photoluminescence, semiconductivity, and proton-hydride interaction between cations NH_4^+ and anions BH_4^-. To this end, we have applied in a controlled way simple concepts such as the tolerance factor and cation/anion substitution. Fig. 2 shows lanthanide-doped $Ca(BH_4)_3$:Eu^{2+} luminescing under the X-ray beam.

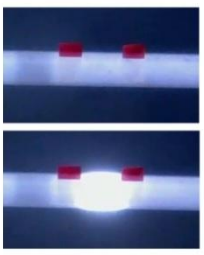

Figure 2. Eu^{2+} luminescence under X-ray excitation. Top: shutter closed, bottom shutter open.

From a crystallographic point of view, highly interesting effects appeared when investigating the transformation sequence of different compounds as a function of temperature. Both octahedral tilts and polar displacements usually tend to vanish as the

superstructure successively does in metal oxide and halide perovskites. Superstructures hence are generated when temperature is decreased, in particular octahedral tilts are easily assigned to soft modes condensing at the zone center.
In $AB(BH_4)_3$ we find that the symmetry-relation between HT-LT phases is very often reversed. Our working hypothesis assigns the origin of this behaviour to interactions between molecular B-H vibrations and lattice phonons. For instance, a very well-known zone boundary instability at the *R*-point of symmetry *Pnma* [3] is activated upon heating $KCa(BH_4)_3$ into the HT-phase (Figure 3). At the transition point the bandwidth of the Raman B-H stretching signature shows a discrete step, which does not occur for another member, $CsCa(BH_4)_3$, whose order-disorder transition does not involve displacements, and hence no lattice instability.

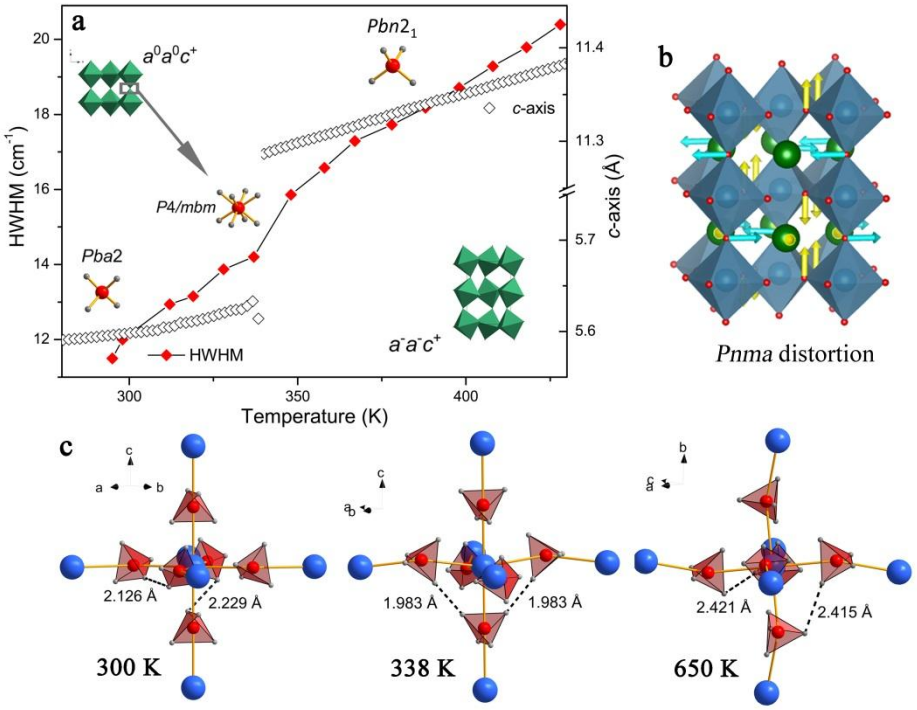

Figure 3. Changes in structure during the high-temperature phase transition of $KCa(BH_4)_3$, followed by *in-situ* powder diffraction at SNBL and Raman spectroscopy (a). The corresponding apolar parent distortion is shown in (b), relevant short H···H contacts within the $Ca(BH_4)_6$-octahedron in (c).

A thorough symmetry analysis was supported by DFT solid state calculations and suggests close homopolar repulsive di-hydrogen contacts to be crucial for the structural behaviour of $AB(BH_4)_3$ (Figure 3). Besides providing a stable borohydride host for functional design, the borohydride perovskite hence implements weak interactions, known from molecular and supramolecular chemistry to a structural behaviour otherwise governed by lattice vibrations. Further evidence for this scheme has in the meantime been provided by quasielastic neutron scattering studies of BH_4 reorientations [4]. This interaction scheme has shown to produce superstructures up to 16-fold in a very basic composition, e.g. $RbCa(BH_4)_3$ (Figure 4).

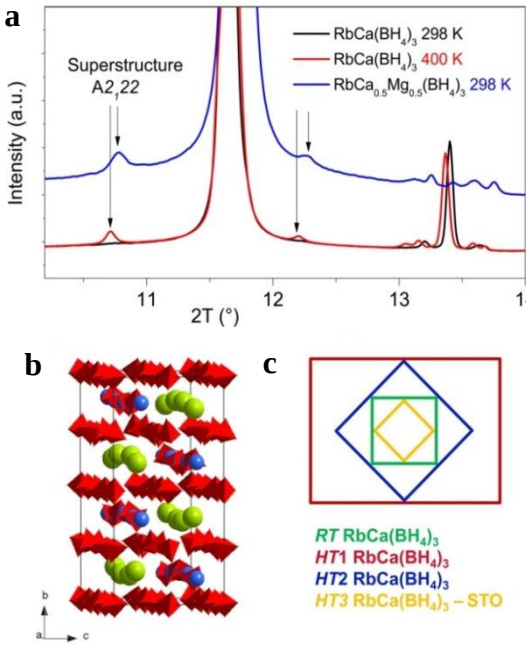

Figure 4. Anomalous high-temperature behaviour of $RbCa(BH_4)_3$, showing in (b) a large superstructure in the *HT* – phase, and its *RT* – stabilization by cation substitution, visible from diffraction data in (a). A schematic unit-cell relationship drawn for the parent-type cubic $SrTiO_3$.

This extensive study on the Pv type in borohydrides has extended the possible applications of metal borohydrides far beyond hydrogen storage. The results from this study have very recently allowed us develop a single crystal growth procedure and grow the first mixed-metal borohydride single crystal, whose structure and transformations were studied at SNBL [5] and confirm the hypotheses developed on powder samples. The perovskites $K_3Gd(BH_4)_6$ and $Cs_3Gd(BH_4)_6$ have shown excellent values for the magnetic entropy change due to the insignificant mixing of wave functions pertaining to BH_4 (molecular orbitals) and Gd (*f*-orbitals) and are currently being evaluated as refrigerants for sub-Kelvin applications [6].

References

[1] David, W. I. F., Faraday Discuss. 151 (2011) 399-414.
[2] P. Schouwink, V. D'Anna, M. B. Ley, L. M. Lawson Daku, B. Richter, T. R. Jensen, H, Hagemann and R, Černý J. Phys. Chem. C 116 (2012) 10829-10840.
[3] J. M. Rondinelli and C. J. Fennie, Adv. Mater. 24 (2012), 1961-1968.
[4] P. Schouwink, H. Hagemann, J. P. Embs, V. D'Anna and R, Černý, (submitted)
[5] P. Schouwink, A. Ramel, E. Giannini and R. Černý, CrystEngComm, 17 (2015), 2682-2689.
[6] P. Schouwink, E. Didelot, T. Mazet and R, Černý, (submitted)

Publication

P. Schouwink P., M. B. Ley, A. Tissot, H. Hagemann, T. R. Jensen,L. Smrčok L. and R. Černý, *Nature Comm*. **5** (2014) 5706.

Reactivity and Synergism of Vanadium in Microporous Supports with Copper as a Co-cation

Katrine Lie Bøyesen, Tina Kristiansen, Karina Mathisen*

Department of Chemistry, Norwegian University of Science and Technology, N-7491 Trondheim Norway

Selective oxidation of propene using molecular oxygen can proceed through different reaction pathways; epoxidation which yields primarily propylene oxide (PO), or allylic oxidation where the unsaturated aldehyde acrolein (CH_2CHCOH) can be formed [1-4]. Acrolein is an important industrial intermediate currently being produced by energy demanding processes, and developing alternate reaction routes for this intermediate is highly topical. Promoted bismuth molybdate catalysts are at present utilised commercially for production of acrolein, with a selectivity reaching 90 % at temperatures 300-400°C [5]. Catalyst lifetime depends greatly on the stability of these catalysts in terms of sintering, which decreases activity and selectivity until catalyst replacement is necessary [5].

In selective oxidation of hydrocarbons, a dynamic reduction and re-oxidation behaviour of the active metal is believed to be crucial [6]. It is therefore important to quantify the valence fractions of copper and vanadium during working conditions during selective oxidation of propene. However, quantifying valence fractions of vanadium species during working conditions has proved to be challenging [7]. We wanted therefore to study the vanadium and copper containing samples with *in situ* XAS, and put special emphasis on methods to quantify the valence fractions.

Additionally, we wanted to study the effect of carrier material, and compared the two 3-D systems of the neutral AlPO-5 (VCu:AlPO-5) and the acidic H-ZSM-5 (VCu:ZSM-5), and to explore possible interactions or synergistic effects. In addition to different acidic properties, these two 3-D supports also have different pore characteristics The zeolite has a 3-D zigzag pore system with pore size of P_d=5.4-5.6 Å, whereas AlPO-5 consist of 1-D channels with pore size P_d=7.3 Å. Figure 1 illustrates the MFI structure of ZSM-5 and the AFI structure of AlPO-5. Choosing three-dimensional supports for catalytically active metal species has several benefits; their large internal surface areas promotes higher metal uptake, and shape selective properties can impose growth limitation on nanoparticles. Several studies report on the dynamic interplay between nanoporous supports and an active metal, which prevents sintering and/or oxide formation and thus increases catalyst lifetime [8-10]. In house catalytic measurements established that VCu:AlPO-5 showed superior activity towards acrolein compared to the monometallic counterparts and the acidic VCu:ZSM-5.

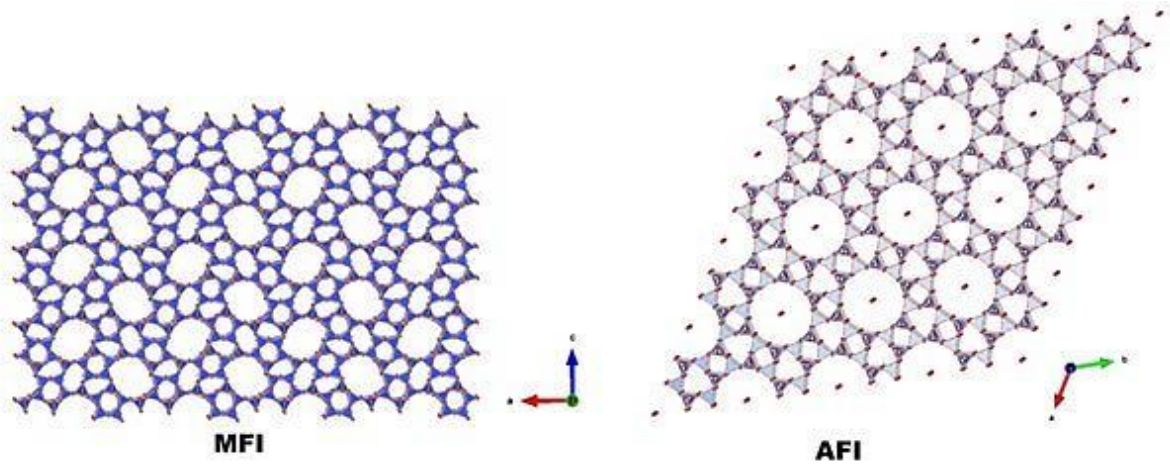

Figure 1 The MFI structure of ZSM-5 and the AFI structure of AlPO-5

In this study, the reducibility and speciation of both metals introduced into the two different pore systems were studied by temperature programmed reduction in propene (C_3H_6-TPR) to 450°C utilising *in situ* XAS combined with *in situ* X-ray Diffraction (XRD). Copper K-edge XAS data and high resolution XRD data were collected at the Swiss-Norwegian Beamlines (SNBL, BM01B) at the European Synchrotron Radiation Facility (ESRF) in transmission mode. Vanadium K-edge data were collected in fluorescence mode at BM01B, SNBL.

The X-ray Absorption Near Edge Spectroscopy (XANES) and Extended X-ray Absorption Fine Structure (EXAFS) part of the XAS spectrum yield information about the nature of the active species. The XANES region for vanadium compounds can give information regarding the oxidation state and local geometry. However, obtaining unambiguous results from XANES can be challenging. The XANES region can be affected by different parameters, which can counteract or amplify each other as seen in Table 1 supported by Figure 2. According to our reference compounds, we found that quantification of the valence fraction at the V K-edge should be done by using the threshold energy, E_0.

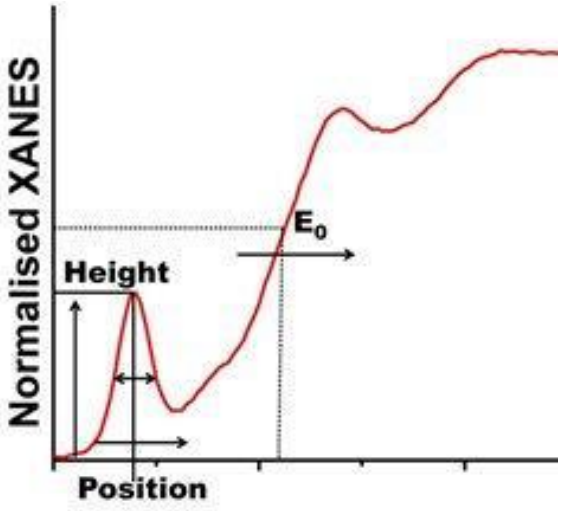

Figure 2 Illustration of how the XANES of vanadium compounds varies

Table 1 An overview how different factors changes the parameters in vanadium XANES

		Increasing valence	Higher degree of symmetry (loss of V=O)	V-O distribution
Abs.edge	E_0	→	←	-
	ΔE	→	←	-
Pre-edge	Height	↑	↓	-
	Width	-	-	↔
	Position	→	-	-

At the Cu K-edge, determination of E_0 is complicated due to different shoulder features arising on the absorption edge. However, the XANES region can be used as a fingerprint method by comparing references and samples which provides a good indication of the valence state. Additionally, linear combination can be applied in order to quantify the valence fraction. However, this requires references with similar chemical surroundings as in the sample. We found the EXAFS region to be more reliable in quantifying the valence fraction using the reduced multiplicities method [11].

Figure 2 shows the *in situ* XANES of VCu:AlPO-5 and the monometallic Cu:AlPO-5 during C_3H_6-TPR.

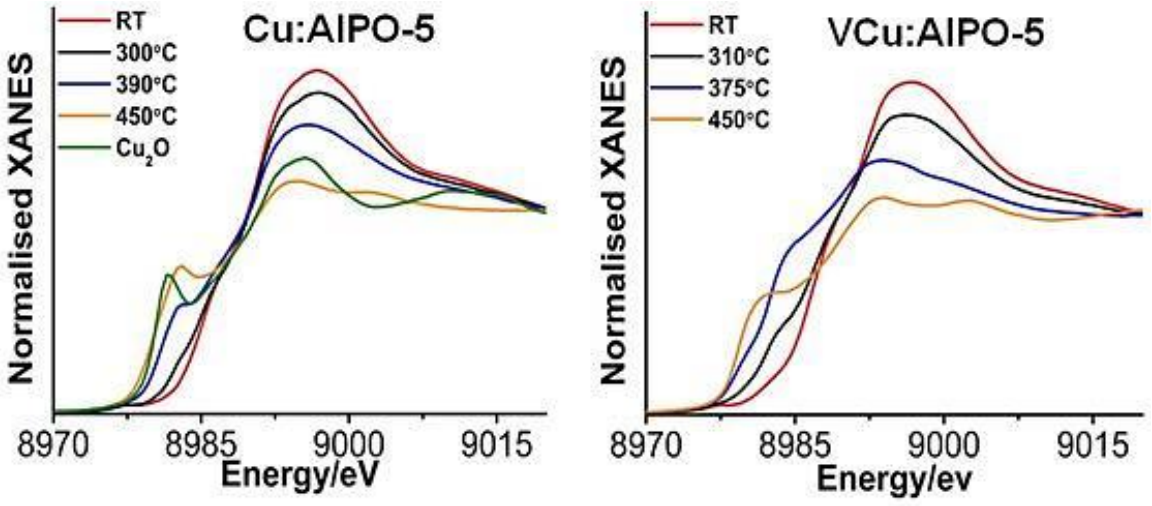

Figure 3 *In situ* XANES of Cu:AlPO-5 and VCu:AlPO-5 during C_3H_6-TPR.

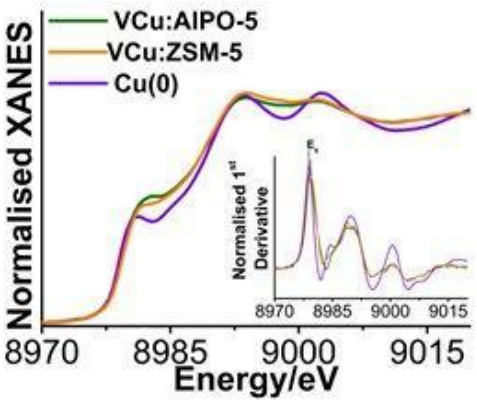

Figure 4 *In situ* XANES of VCu:AlPO-5 and VCu:ZSM-5 compared to the metallic copper reference

As seen in Figure 2, the major species present in Cu:AlPO5 is Cu(I), whereas the major species present in VCu:AlPO-5 is Cu(0). Figure 3 shows *the in situ* XANES of VCu:AlPO-5 compared to VCu:ZSM-5 and the metallic reference. For both the neutral AlPO-5 and acidic ZSM-5 vanadium promotes formation of metallic copper in propene.

Interestingly, *in situ* EXAFS at 450°C in propene revealed that the copper clusters had a particle size of 6.4 Å in the neutral AlPO-5, and 12 Å in the acidic ZSM-5. The average size of the metallic copper clusters is too large for the pores in ZSM-5, indicating that they reside on the external surface of the zeolite, whereas they are small enough for the pore aperture in AlPO-5. This study indicates that shape selectivity introduces growth limitations on the copper clusters.

The reversible redox behaviour was also studied by cycling the samples between oxygen at propene at 450°C. High resolution XRD revealed a fraction of the metallic clusters formed larger crystallites on the external surface (Figure 4), not present in oxygen treatments or the propene/O_2 reaction mixture for both samples (VCu:AlPO-5 and VCu:ZSM-5).

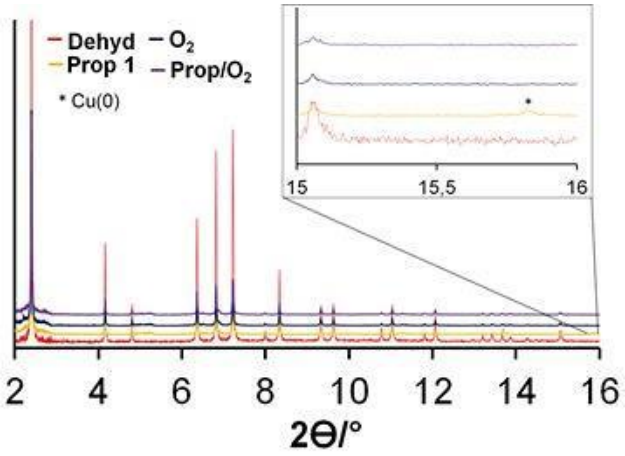

Figure 5 PXRD for VCu:AlPO-5 during cycling at 450°C; inset the area where metallic copper is detected at 15.8°.

These findings show that introducing both copper and vanadium into AlPO-5 and H-ZSM-5 greatly affects both activity and selectivity towards acrolein during propene oxidation; however, a neutral carrier is favoured. Additionally the presence of vanadium promotes hyper reduction to metallic copper in VCu:AlPO-5 and VCu:ZSM-5 despite very mild reducing conditions (1 % propene), while the monometallic samples only forms Cu(I) at this temperature. To our knowledge, this is the first *in situ* proof of metallic copper formed during C_3H_6-TPR at very mild conditions. The re-dispersion of the metallic copper clusters was observed for both VCu:AlPO-5 and VCu:ZSM-5, showing reversible catalytic behaviour which might increase the catalyst lifetime.

References:

[1] T.A. Nijhuis, M. Makkee, J.A. Moulijn, B.M. Weckhuysen, *Ind. Eng. Chem. Res.* **45** (2006) 3447-3459.
[2] O.P.H. Vaughan, G. Kyriakou, N. Macleod, M. Tikhov, R.M. Lambert, *J. Catal*. **236** (2005) 401-404.
[3] Y. Wang, H. Chu, W. Zhu, Q. Zhang, *Catal. Today* **131** (2008) 496-504.
[4] W. Zhu, Q. Zhang, Y. Wang, *J. Phys. Chem. C* **112** (2008) 7731-7734.
[5] H.F. Rase, Handbook of Commercial Catalystst, Heterogeneous Catalysts, Handbook of Commercial Catalystst, Heterogeneous Catalysts, CRC Press, Florida, 2000, pp. 260-263.
[6] A. Andersson, *J. Catal*. **69** (1981) 465-474.
[7] B.M. Weckhuysen, D.E. Keller, *Catal. Today* **78** (2003) 25-46.
[8] T. Kristiansen, J.A. Støvneng, M.-A. Einarsrud, D.G. Nicholson, K. Mathisen, *J. Phys. Chem. C* **116** (2012) 20368−20379.
[9] L. Guczi, I. Kiricsi, *Appl. Cata.*, **A186** (1999) 375-394.
[10] K. Mathisen, M.H. Nilsen, C. Nordhei, D.G. Nicholson, *J. Phys. Chem. C* **116** (2011) 171-184.
[11] K. Mathisen, D.G. Nicholson, M. Stockenhuber, *Microporous Mesoporous Mat.* **84** (2005) 261-274.

Publication:

K.L.Bøyesen, T. Kristiansen, K. Mathisen, *PCCP*, **16** (2014) 20451-20463

STATUS OF FACILITY

BM01A

While initially the emphasis on BM01A was on the investigation of pharmaceutically relevant materials, the main focus of activity is now strongly oriented towards energy-related research. Instrumentation development targeted at *in-situ* experiments has also been an important aspect of the beamline work in recent years, particularly for studying catalytic reactions and hydrogen storage. The image plate system has been replaced in May 2012 by a hybrid pixel array detector of the latest generation (a PILATUS 2M detector supplied by Dectris Ltd, Baden) mounted on a very flexible and versatile diffraction platform. Most of the development activities in 2013-2014 have been concentrated on exploiting the full potential of the new detector. The diffractometer equipped with the PILATUS detector is shown in Fig. 1, where the special setup shown in the photograph has been optimized for in-situ powder diffraction measurements. In this case, the user group from Stavanger University was investigating the adsorption of gases on a zeolite.

A recent example of the use of the PILATUS@SNBL for powder diffraction measurements has been reported by Pascal Schouwink et al. from the University of

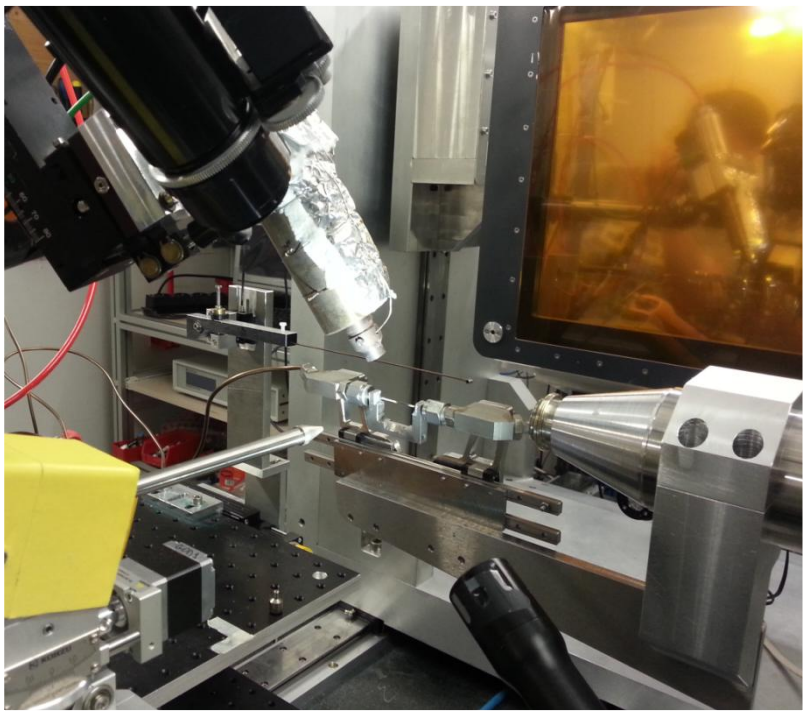

Figure 1. Layout of the new Pilatus2M pixel detector showing the setup optimized for *in-situ* powder diffraction.

Geneva [*Nature Communications*, **5,** 5706 (2014)]. Although conceived as an area detector for protein crystallography experiments, the Pilatus2M pixel detector turns out to be very well suited for powder as well as single crystal diffraction experiments. The Geneva group used BM01A (and other synchrotron beamlines) to characterize a series of 30 new hydride perovskite-like materials. The short data collection times and the extremely rapid read-out cycle made PILATUS@SNBL particularly useful for characterizing the complex temperature dependence of the structures of $KCa(BH_4)_3$, which revealed a series of crystallographic phase transitions.

One of the scientific areas for which the new equipment provides significant advantages is the investigation of diffuse X-ray scattering in single crystals. For example, a group led by Alexander Tagantsev from the Ceramics Laboratory of EPFL has investigated the lattice dynamics of antiferroelectric lead zirconate using inelastic and diffuse X-ray scattering techniques and Brillouin light scattering [*Nature Communications*, **4**, 2229 (2013)]. The results reported by Tagantsev et al. resolve the mystery of the origin of antiferroelectricity in lead zirconate and suggest an approach to the treatment of complex phase transitions in ferroics. An elegant study of the effects of pressure on the diffuse scattering in a single crystal of $Pb(Mg_{1/3}Nb_{2/3})O_3$, called PMN, was reported by a collaborating group from SNBL and ESRF beamline staff [*Z. Kristallogr***.** 2014; **229**(3): 223–229]. Once again, the subject of study was a ferroelectric material. They were able to reveal the pressure evolution of the diffuse scattering quantified in the form of the reconstructed reciprocal space layers. They showed, in agreement with previous observations, that relaxor-specific diffuse scattering disappears under pressure. They also quantified the pressure dependence of the anisotropy of diffuse scattering. Finally, they discussed the appearance of new Bragg reflections, superposed with the diffuse maxima, and related it to the positioning of the relaxor state in a specific region of the perovskite phase diagram.

The combination of high brilliance and high x-ray energies provided by the bending magnet source at the ESRF also allows the users of SNBL to investigate the effects of high pressure on powders using diamond anvil cells. A most unexpected and puzzling phenomenon that can be observed under high pressure, is negative linear

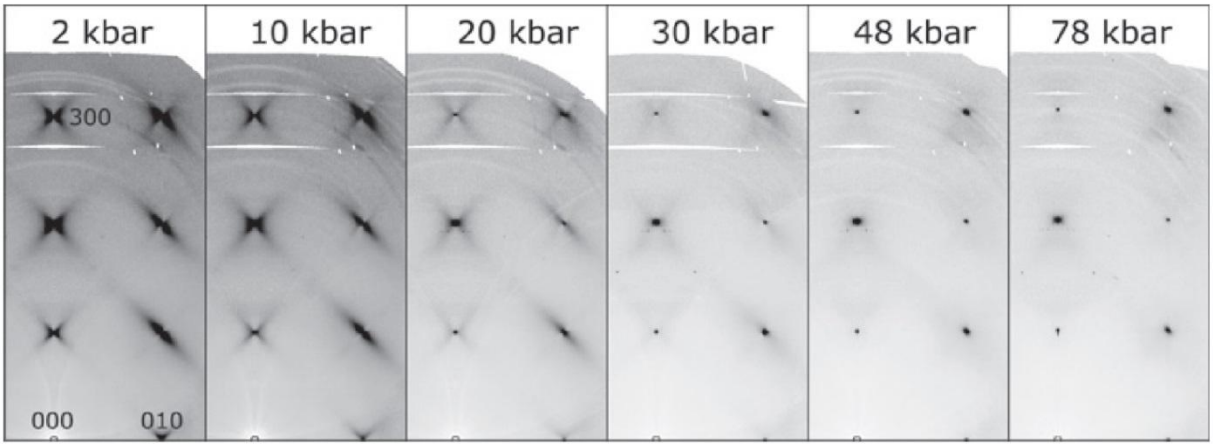

Figure 2. Pressure dependence of diffuse scattering in the *HK0* reciprocal space layer in PNM

compressibility. In a collaboration between the beamline staff and the University of Oxford [Andrew B. Cairns et al., *Nature Materials*, **12**, 212–216 (2013)] it was possible to reveal that the molecular framework material $Zn[Au(CN)_2]_2$ exhibits the most extreme and persistent negative linear compressibility behavior yet reported: under increasing hydrostatic pressure its crystal structure expands in one direction at a rate that is an order of magnitude greater than the typical contraction observed for common engineering materials. In these and similar studies, it is the combination of the excellent characteristics of the source and the high performance of the new generation of pixel detectors that opens up many exciting avenues of research in the fields of solid state physics and crystal chemistry using synchrotron radiation.

Future developments on the beamline

The relocation of BM01B onto another bending magnet port of the ESRF (BM31) will have major implications for the operation of BM01A. Once the B-station hutch has been vacated, we propose to move the KM6 diffractometer into the empty space. As part of this upgrade, we are now equipping the KM6 diffractometer with new motor controls and software which are compatible with the ESRF standards.
We will then operate the two experimental hutches in series, sharing the time of access to the beam provided by the BM01 port. This is common practice at the ESRF, particularly for the CRGs in which several different techniques are often supported on the same beamline. In this way, we will also be properly prepared for the major upgrade of the ESRF planned for 2018-2020. After this upgrade, the opening angle of the available beam from a bending magnet port will be drastically reduced and only the serial mode of operation with two stations will be possible.
Concerning the further development of PILATUS@SNBL, considerable effort is now focused on the organization, processing and storage of the very large amounts of data generated by a typical experiment. In order to define precisely the extent of the problem, and the demands on new software required for streamlined data processing, a joint ESRF/SNBL workshop (“Big data for small molecule crystallography”) will be held early in 2015. Without the proper combination of hardware and software, it will be difficult to exploit the full potential of the new generation of pixel detectors. In another area of technical improvements, the staff of SNBL is collaborating with Dectris Ltd. in an effort to determine the optimum count-rate corrections which should be applied to pixel detector. A joint publication on this subject will shortly appear in the *Journal of Synchrotron Radiation*.

Collaboration between SNBL and external groups

The Memorandum of Understanding (MoU) with the Dutch-Belgian beamline has continued to provide a useful mechanism for the sharing equipment and manpower, and for the exchange of beamtime between the two CRGs. Another MoU has been in existence for several years between SNBL and MaxLab in Sweden. Recently, a group from the BALDER beamline under construction at MAX IV visited SNBL, and discussions about further collaboration between the two laboratories are now in progress.

BM01B

BM1B Powder Diffraction and EXAFS

Scientific results and Current status

After the big infrastructure changes in the 2011 and 2012, during the last two years the station has concentrated on continuing its successful operation. The scientific results are building upon the availability of excellent data quality of both the diffraction and absorption techniques. The setup on this station is extremely flexible and allows for rapid alternations between the various techniques. Our visiting user groups extensively use these opportunities in order to reveal structure-functional relationships using long and short range information from their samples collected using *in-situ* experiments. Most (>80%) of the materials studied on the beamline have targeted applications in: catalysis, energy storage, sensors and environmental sciences. Despite the strong *in-situ* capabilities of this station the more traditional *ex-situ* experiments have not suffered in terms of data quality, and continue to provide outstanding results. A good illustration of such work was done by Smeets *et al.*[1], published in *Angewante Chemie* who synthesized and solved the structure of a new high silica Zeolite with a combination of *High Resolution Powder Diffraction* and Electron Microscopy. Such studies provide fundamental structural information on new zeolites, potentially enabling the insertion of catalytic centers to create fascinating properties. Another good example, using *EXAFS* this time, was published in *Nature Communications* by Blazina *et al*.[2] which deals with the understanding of the worldwide distribution of selenium in soils and crops. As selenium is an essential trace element needed for human health, it is important to understanding the mechanisms which govern its distribution and thus enabling the prediction of Se depleted areas in the world. This, in turn, potentially allows preventive measures to be taken in order to avoid human health hazards.
No major changes have been made recently to the equipment, and the new end-station, build during the long ESRF shutdown on 2011-2012, has proven its enhanced operational efficiency (see Figure 3).

Figure 3. BM01B end-station

Future developments on the beamline

The major development, using a substantial part of both financial and human resources, is the planned move of BM01B to an empty bending magnet port on the ESRF storage ring. In mid 2016 the whole BM01B beamline will be operating from its *own* independent bending magnet port on a completely new infrastructure. The design of the new infrastructure is well under way and shown in Figure 4.

The new implementation will allow the former SNBL B-station (renamed as BM31), to continue its operation after the ESRF source upgrade in 2018. This would not have been possible with the existing shared operation together with BM01A on one common ESRF bending magnet port. The planned new source - a multipole wiggler instead of a bending magnet- will be installed during the 2018/19 ESRF upgrade. It will increase the flux on the sample by at least a factor of two already without modifications to the x-ray optics. The extra space available on the new beamline also enables the development of optimized optical schemes and new detector systems to be implemented around the sample. Design studies are currently being made to fully exploit the new space in the future. The infrastructure work has already advanced sufficiently such that the first orders are about to be placed.

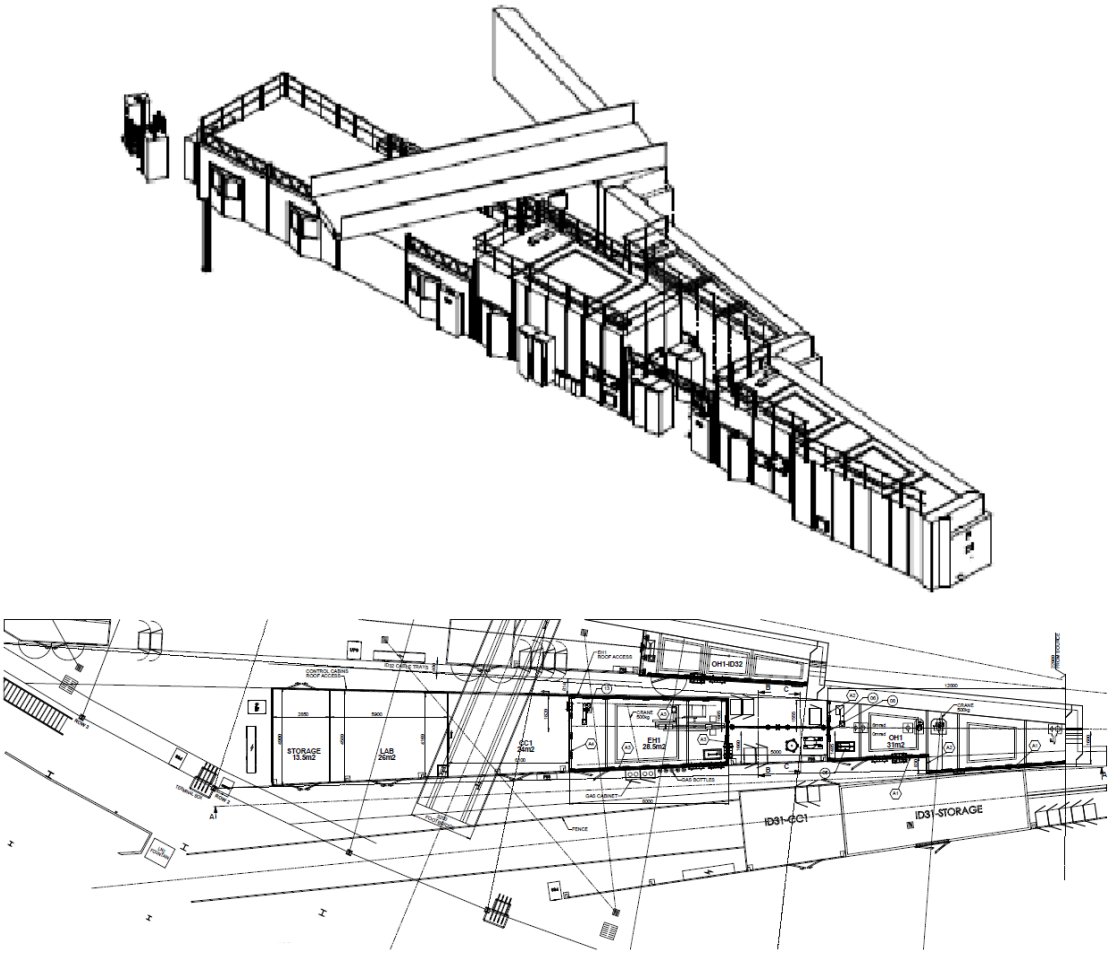

Figure 4. The new BM31 infrastructure

Collaborations between SNBL and external groups

Collaborations are a very important part of the activities at SNBL, as it is often beneficial for many of the users of the beamline. The results often reach out to a significant part of the SNBL or synchrotron community, as explained below. Hence several formal collaborations have been established between beamline staff and user groups providing both additional funding and manpower. More precisely, an international collaboration between the Norwegian University of Science and Technology ***NTNU*** in Trondheim, the Institute of Chemical Research Catalonia ***ICIQ*** in Tarragona and SNBL is now in full swing. This collaboration has funded the 12 million pixel CMOS detector (Abdala *et al.*)[3] for fast diffraction, complementing the station such that EXAFS and powder diffraction measurements can now be performed on the same times scale (a few ~10s). On the same project, chemometric data analysis tools are currently being adapted for absorption measurements to efficiently exploit the enormous data streams coming from SNBL these days (Voronov *et al.*)[4]. This will not only serve the SNBL user community but has potentially a much wider impact.

The new diffraction capabilities are now successfully exploited on daily basis by many of the users of this station, the project has also triggered a follow up collaboration between the "Foundation for Scientific and Industrial Research", ***SINTEF***, the University of Oslo ***UIO*** and SNBL. This collaboration intends to further develop the use of the CMOS detection system for Total Scattering experiments at SNBL. In this context the combination of the newly installed focusing 2nd crystal for high energies, providing one order of magnitude more flux on the sample, and the CMOS detector are potentially a perfect match. First results are very promising and analysis in ongoing.

Informal collaborations between beamline staff and Swiss and Norwegian users groups occur naturally as part of the activities on the beamline. These collaborations are especially fruitful when specialized sample environmental cells have to be developed. Such projects need to take into account a complex set of boundary conditions both for the chemical process in question but also for the x-ray diffraction and absorption characteristics of sample and compatible window materials. Hence the know-how of both beamline scientist and user groups has to be combined. A successful project between ***UIO*** and SNBL has led to the development of an automated sample changer for electrochemistry now already available to all users (see Figures 5-6). Furthermore there has been some software development to combine the battery-related data measured by a galvanostat, with the beamline data into the same file. This ensures a perfect temporal match between the electro-chemical information (e.g. the charge state of the battery) and the X-ray data such as XANES (i.e. to probe the valence state of a given element) and powder diffraction (to gather structural information on the electrode materials).

Another good example is a collaboration between the Eidgenössische Technische Hochschule Zürich ***ETHZ*** and SNBL resulting in high rank publications in *Chemistry of Materials* (Hirsch *et al.* and Staniuk *et al*)[5,6] and *Nanoscale* (Kranzlin *et al.*)[7]. This collaboration deals with the elucidation of production processes by in situ crystallization studies on battery and sensor materials. An electrochemistry cell has also successfully been developed in collaboration with the Paul Scherrer Institute in Villingen ***PSI,*** and SNBL. The authors combined in-situ low energy titanium absorption measurements, already complex in itself, and high energy diffraction studies on a working battery which has led to a publication in *J.Phys Chem C*. Another collaboration between the Southern Federal University in Rostov ***SFedU*** (Russia), ***Turin University***, the ***ETHZ***, Swiss Light

Source ***SLS*** and SNBL has produced an impressive work presenting theoretical models predicting the XANES features with *matching* experimental data on supported palladium nanoparticles during temperature and pressure dependent hydrogen concentration variations (Bugaev *et al.)*[8].

It is clear that close collaborations between users and beamline staff enable users to make use of the full potential provided by the SNBL. The results of such projects often reach out to other parts of the user community making it a very satisfactory way to achieve important technical progress.

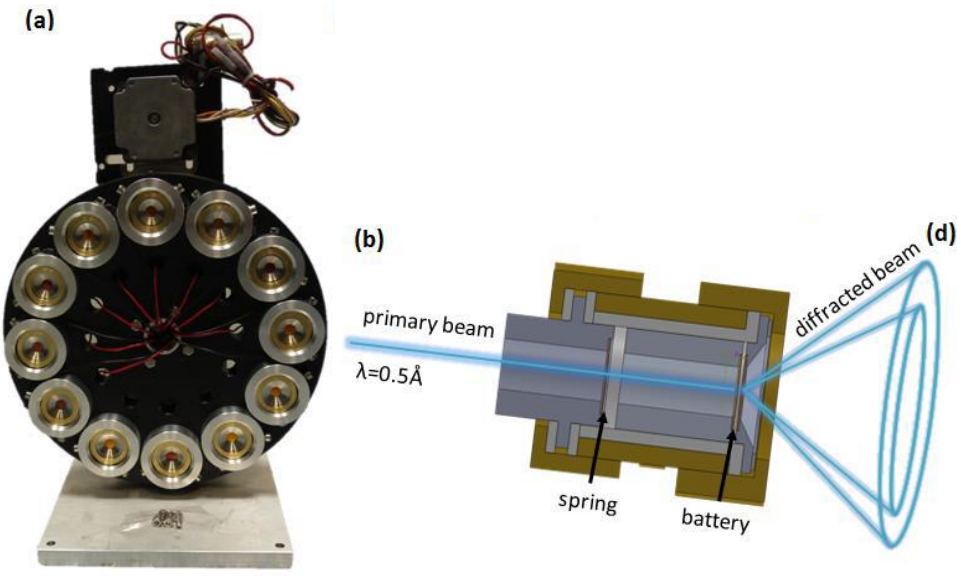

Figure 5. Automated battery changer (a) and electrochemistry cell for diffraction (b).

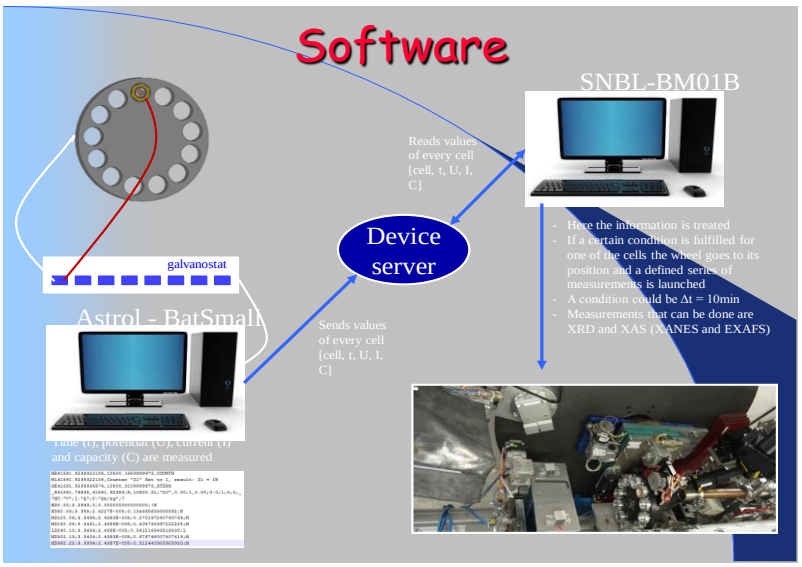

Figure 6. SNBL data acquisition software, exchanging data with the galvanostat controller via a "device server"

References:

1) Smeets, S., Xie, D., Baerlocher, Ch., McCusker, L.B., Wan, W., Zou, X., Zones, S.I. *High-Silica Zeolite SSZ-61 with Dumbbell-Shaped Extra-Large-Pore Channels* Angewandte Chemie, 126, 39, 10566-10570, 2014

2) Blazina, T., Sun, Y., Voegelin, A., Lenz, M., Berg, M., Winkel, L.H.E. *Terrestrial selenium distribution in China is potentially linked to monsoonal climate* Nature Communications 5, Article number: 4717, 2014

3) Abdala, P. M., Mauroy, H., Van Beek, W. *A large-area CMOS detector for high-energy synchrotron powder diffraction and total scattering experiments* J. Appl. Cryst., 47, 449-457, 2014

4) Voronov, A., Urakawa, A., Van Beek, W., Tsakoumis, N.E., Emerich, H., Rønning, M. *Multivariate curve resolution applied to in situ X-ray absorption spectroscopy data: An efficient tool for data processing and analysis* Analytica Chimica Acta, 840, 20, 20-27, 2014

5) Hirsch, O., Zeng, G., Luo, L., Staniuk, M., Abdala, P.M. et al. *Aliovalent Ni in MoO_2 Lattice— Probing the Structure and Valence of Ni and Its Implication on the Electrochemical Performance* Chem. Mater., 26, 15, 4505-4513, 2014

6) Staniuk, M., Hirsch, O., Kränzlin, N., Böhlen, R., Van Beek, W., Abdala, P.M., Koziej, D. *Puzzling Mechanism behind a Simple Synthesis of Cobalt and Cobalt Oxide Nanoparticles: In Situ Synchrotron X-ray Absorption and Diffraction Studies* Chem. Mater., 26, 6, 2086–2094, 2014

7) Kranzlin, N., Staniuk, M., Heiligtag, F. J., Luo, L., Emerich, H., Van Beek, W., Niederbergera, M., Koziej, D. *Rationale for the crystallization of titania polymorphs in solution* Nanoscale, 6, 14716-14723, 2014

8) Bugaev, A.L., Guda, A.A., Lomachenko, K.A., Srabionyan, V.V., Bugaev, L.A., Soldatov, A.V., Lamberti, C. et al. *Temperature- and Pressure-Dependent Hydrogen Concentration in Supported PdHx Nanoparticles by Pd K-Edge X-ray Absorption Spectroscopy* J. Phys. Chem. C, 118, 19, 10416-10423, 2014

SNBL - FACTS AND FIGURES

BUDGET (in kCHF)

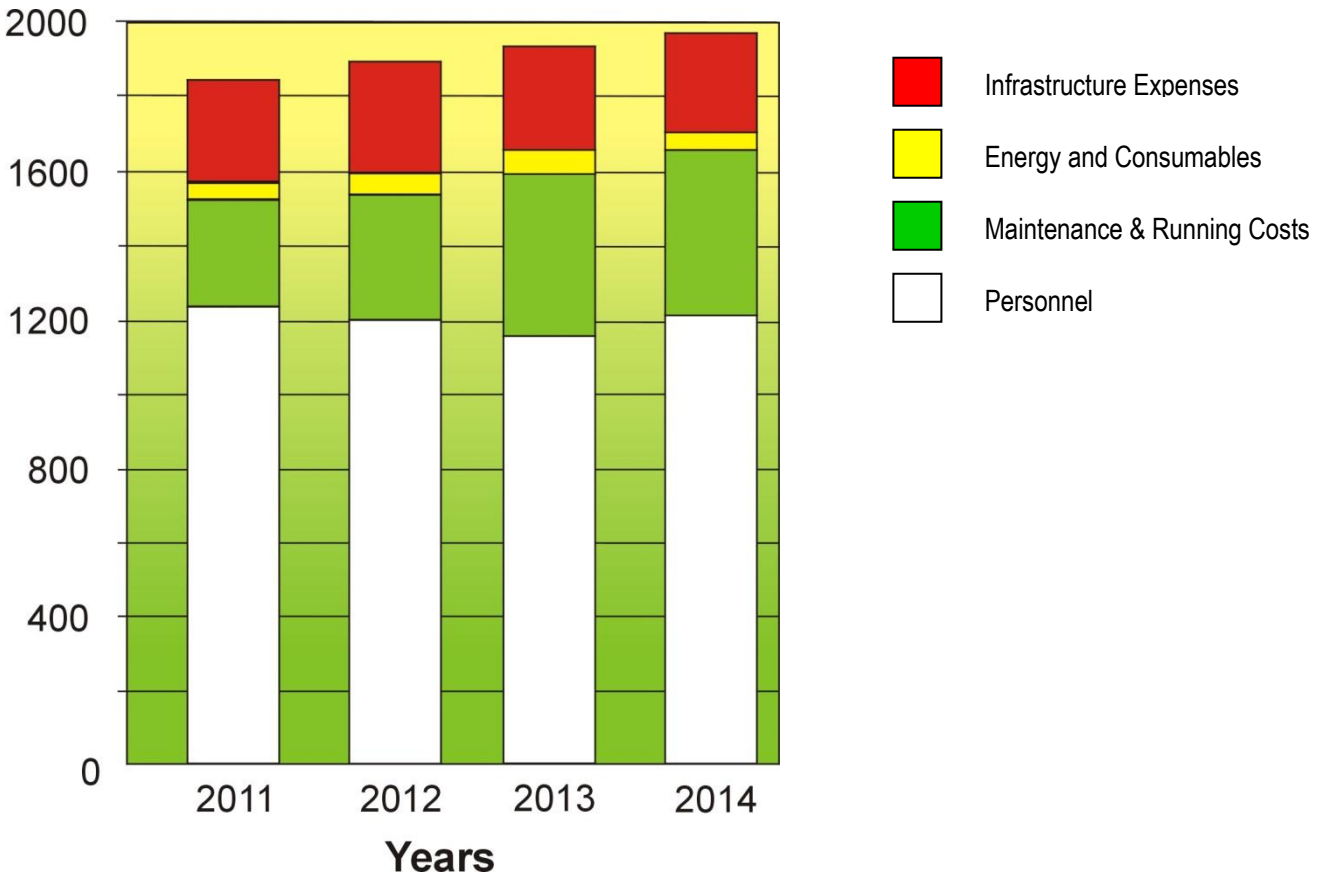

BUDGET in kCHF	2011	2012	2013	2014
Personnel	1,230	1,207	1,155	1,208
Maintenance and Running Costs	300	339	450	438
Energy and Consumables	55	60	59	60
Infrastructure Expenses	250	283	262	267
TOTAL	**1,835**	**1,790**	**1,925**	**1,972**

INCOME (in kCHF)

Income Outside Contract

Income According to Contract

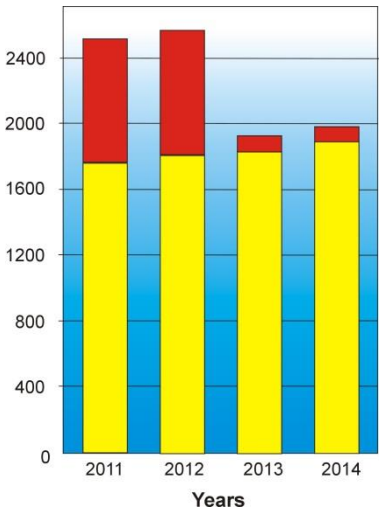

INCOME in kCHF	2011	2012	2013	2014
Income According to Contract	1,750	1,794	1,850	1,900
Income Outside Contract	760	796	72	72
TOTAL	**2,510**	**2,590**	**1,930**	**2,000**

EXPENDITURE (in kCHF)

Infrastructure Expenses

Energy and Consumables

Maintenance & Running Costs

Personnel

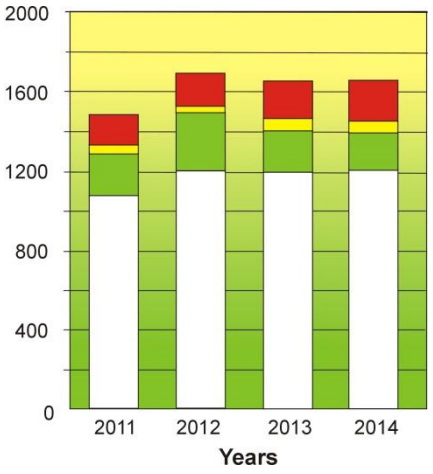

EXPENDITURE in kCHF	2011	2012	2013	2014
Personnel	1,082	1,213	1,192	1,208
Maintenance and Running Costs	208	276	225	195
Energy and Consumables	41	34	50	49
Infrastructure Expenses	155	169	184	202
TOTAL	**1,486**	**1,692**	**1,651**	**1,654**

Organization Chart of the SNBL

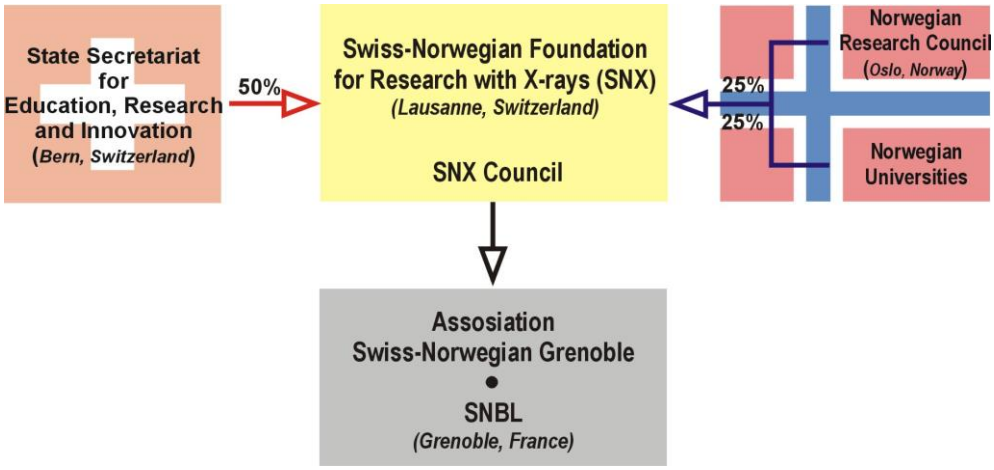

SNX Council

MEMBERS

Prof. G. Chapuis – Chairman	EPF Lausanne, Switzerland
Prof. H.Fjellvag – Vice-Chairman	University of Oslo, Norway
Prof. M.Ronning	NTNU, Trondheim, Norway
Prof. J. van Bokhoven	ETH Zurich / PSI, Switzerland
Prof. P.Macchi	University of Bern, Switzerland
Prof. B.Hauback	IFE, Kjeller, Norway
Dr. V. Dmitriev	SNBL, Grenoble, France

ADVISERS

Dr. B. Jacobsen	The Research Council of Norway
Dr. M. Steinacher	State Secretariat for Education, Research and Innovations, Switzerland

SNBL Staff

(2013-2014)

Dr. V. Dmitriev – Project Director

A-station	*B-station*
Dr. P. Pattison – BL responsable	**H. Emerich** – BL responsable
Dr. D. Chernyshov – BL scientist	**Dr. W. van Beek** – BL scientist
Dr. V. Dyadkin – BL scientist	**Dr. P. Abdala** – BL scientist

Ch. Heurtebise – Administrative manager

G. Wiker – Senior technician

PUBLICATIONS

Publication Rate since start-up of SNBL

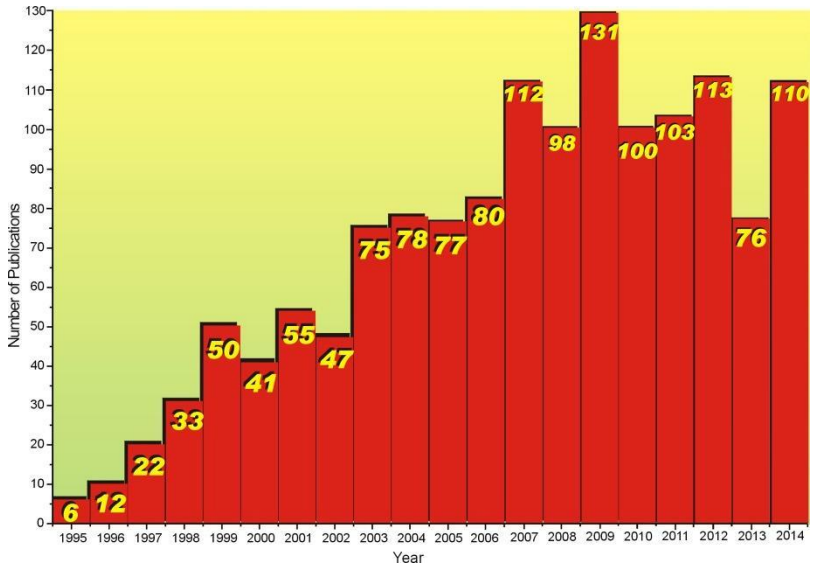

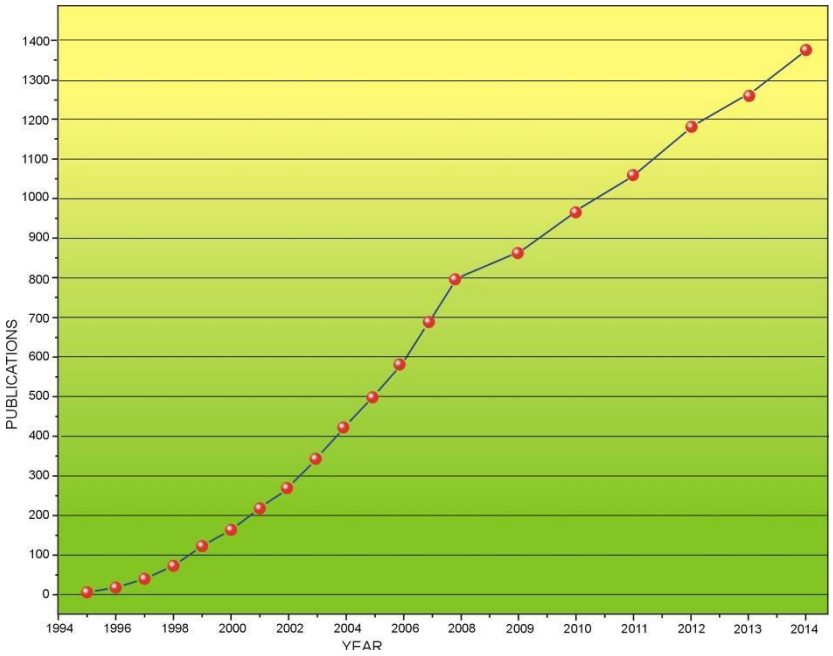

List of Publications

2013

1. **Allieta, M.., Scavini, M., Lo Presti, L., Coduri, M., Loconte, L., Cappelli, S., Oliva, C. et al.** *Charge ordering transition in $GdBaCo_2O_5$: Evidence of reentrant behavior* Phys. Rev. B **88**, 214104-214114, 2013
2. **Andrault, D., Antonangeli, D., Dmitriev, V., Filinchuk, Y., Hanfland, M., Hazemann, M., Krisch, M. et al.** *Science under Extreme Conditions of Pressures and Temperatures at the ESRF* Synchrotron Radiation News, **26**, 5, 2013
3. **Arakcheeva, A., Ashokkumar, S., Leela, S., Ramamurthi, K., Stoeckli-Evans, H. et al.** *Synthesis, growth and characterization of 4-bromo-4'nitrobenzylidene aniline (BNBA): A novel nonlinear optical material with a (3+1)-dimensional incommensurately modulated structure* CrystEngComm, **15**, 2474-2481, 2013
4. **Arakcheeva, A., Pattison, P., Bauer-Brandl, A., Birkedal, H., Chapuis, G**. *Cimetidine, $C_{10}H_{16}N_6S$, form C: crystal structure and modelling of polytypes using the superspace approach* J. Appl. Cryst., **46**, 99-107, 2013
5. **Aree, Th., Buergi, H.-B., Minkov, B.S., Boldyreva, E.V., Chernyshov, D., Tornroos, K.W.** *Dynamics and Thermodynamics of Crystalline Polymorphs. Part 2:* β *-Glycine, Analysis of Variable-Temperature Atomic Displacement Parameters* J. Phys. Chem. A, **113**, 33, 8001-8009, 2013
6. **Barpanda, P., Ati, M., Melot, B., Chotard, J.-N., Rousse, G., Tarascon, J.-M.** *Effect of Both Mn and Zn Partial Substitution on the Electrochemical Performance of $LiFeSO_4F$* ECS Trans., **45**, 29, 227-233, 2013
7. **Barzan, C., Gianolio, D., Groppo, E., Lamberti, C., Monteil, V. et al.** *The Effect of Hydrosilanes on the Active Sites of the Phillips Catalyst: The Secret for In Situ* α*-Olefin Generation* Chemistry - A European J., **19**, 51, 17277–17282, 2013
8. **Cairns, A.B., Catafesta, J., Levelut, C., Rouquette, J., Van der Lee, A., Peters, L., Thompson, A.L., Dmitriev, V. et al.** *Giant negative linear compressibility in zinc dicyanoaurate* Nature Materials, **12**, 212-216, 2013
9. **Can, M., Krucinska, J., Zoppellaro, G., Andersen, N.H., Wedekind, J.E., Hersleth, H.-P. et al.** *Structural Characterization of Nitrosomonas europaea Cytochrome c-552 Variants with Marked Differences in Electronic Structure* ChemBioChem., **14**, 14, 1828-1838, 2013
10. **Chakraborty, P., Tissot, A., Peterhans, L., Guénée, L., Besnard, C., Pattison, Ph., Hauser, A.** *Determination of the molecular structure of the short-lived light-induced high-spin state in the spin-crossover compound $[Fe(6\text{-}mepy)_3tren](PF_6)_2$* Phys. Rev. B **87**, 214306-214315, 2013
11. **Cerny, R., Schouwink, P., Sadikin, Y., Stare, K., Smrcok, L., Richter, B., Jensen, T.R.** *Trimetallic Borohydride $Li_3MZn_5(BH_4)_{15}$ (M = Mg, Mn) Containing Two Weakly Interconnected Frameworks* Inorg. Chem., **52**, 17, 9941–9947, 2013
12. **Chevreau, H., Devic, Th., Salles, F., Maurin, G., Stock, N., Serre, Ch.** *Mixed-Linker Hybrid Superpolyhedra for the Production of a Series of Large-Pore Iron(III) Carboxylate Metal–Organic Frameworks* Angewandte Chemie Int. Ed., **52**, 19, 5056-5060, 2013
13. **Collings, I.M., Cairns, A.B., Thompson, A.L., Parker, J.E., Tang, C.C., Tucker, M.G., Catafesta, J. et al.** *Homologous critical behaviour in the molecular frameworks $Zn(CN)_2$ and $Cd(imidazolate)_2$* J. Am. Chem. Soc., **135**, 20, 7610-7620, 2013
14. **Conterosito, E., Croce,G., Palin, L., Perioli, L.et al.** *Structural characterization and thermal and chemical stability of bioactive molecule/hydrotalcite (LDH) nanocomposites* Phys. Chem. Chem. Phys., **15**, 13418-13433, 2013
15. **Conterosito, E., Van Beek, W., Palin, L., Croce, G., Perioli, L. et al.** *Development of a fast and clean intercalation method for organic molecules into Layered Double Hydroxides* Cryst. Growth Des., **13**, 3, 1162-1169, 2013

16. **Deka, U., Lezcano-Gonzalez, I., Warrender, S.J., Picone, A.L., Wright, P.A. et al.** *Changing active sites in Cu–CHA catalysts: deNOx selectivity as a function of the preparation method* Microp. & Mesop. Mater., **166**, 144-152, 2013
17. **Doronkin, D.E., Fogel, S., Gabrielsson, P., Grunwaldt, J.-D., Dahl, S.** *Ti and Si doping as a way to increase low temperature activity of sulfated Ag/Al_2O_3 in H_2-assisted NH_3-SCR of NO_x* Applied Catalysis B: Environmental, **148-149**, 62–69, 2013
18. **Engelke, J ., Menzel, D., Dyadkin, V. A.** *Thin film MnGe grown on Si(111)* J. Phys.: Condens. Matter, **25**, 472201-472206, 2013
19. **Falch, T.L., Floystad, J.B., Breiby, D.W., Elster, A.C.** *GPU-Accelerated Visualization of Scattered Point Data* Access, IEEE, **1**, 564 - 576 , 2013
20. **Gianolio, D., Vitillo, J G., Civalleri, B., Bordiga, S., Olsbye, U., Lillerud, K. P., Valenzano, L., Lamberti, C.** *Combined study of structural properties on metal-organic frameworks with same topology but different linkers or metal* J. Phys.: Conf. Ser. **430**, 012134-012140, 2013
21. **Gorfman, S., Schmidt, O., Tsirelson, V., Ziolkowski, M., Pietsch, U.** *Crystallography under External Electric Field* Zeitschrift für anorganische und allgemeine Chemie, **639**, 11, 1953-1962, 2013
22. **Grebenev, V.V., Makarova, I. P., Ksenofontov, D. A., Komornikov, V. A., Dmitricheva, E. V.** *Phase transitions in $Cs_5(HSO_4)_2(H_2PO_4)_3$ crystal* Crystallography Reports, **58**, 6, 894-898, 2013
23. **Grigoriev, S. V., Potapova, N.M., Siegfried, S.-A., Dyadkin, V. A., Moskvin, E. V., Dmitriev, V., Menzel, D. et al.** *Chiral Properties of Structure and Magnetism in $Mn_{1-x}Fe_xGe$ Compounds: When the Left and the Right are Fighting, Who Wins?* Phys. Rev. Lett., **110**, 207201-207206, 2013
24. **Hammer, N., Mathisen, K., Rønning, M.** *CO Oxidation over Au/TiO_2–Carbon Catalysts: The Effect of Thermal Treatment, Stability and TiO_2 Support Structure* Topics in Catalysis, **56**, 9-10, 637-649, 2013
25. **Hennig, Ch., Ikeda-Ohno, A., Kraus, W., Weiss, S., Pattison, P., Emerich, H., Abdala, P.M., Scheinost, A.C.** *Crystal Structure and Solution Species of Ce(III) and Ce(IV) Formates: From Mononuclear to Hexanuclear Complexes* Inorg. Chem., **52**, 20, 11734–11743, 2013
26. **Hermann, D., Emerich, H., Lepski, R., Schaniel, D., Ruschewitz, U.** *Metal–Organic Frameworks as Hosts for Photochromic Guest Molecules* Inorg. Chem., **52**, 5, 2744-2749, 2013
27. **Itoi, M., Maurin, I., Varret, F., Frye, F.A., Talham, D.R., Chernyshov, D., Boukheddaden, K.** *When local deformations trigger lattice instability: Flow diagram investigations for photoinduced and quenched metastable states in a Prussian blue analog* Phys. Rev. B **88**, 094104-094111, 2013
28. **Kaegi, R., Voegelin, A., Ort, Ch., Sinnet, B., Thalmann, B., Krismer, J., Hagendorfer, H. et al.** *Fate and Transformation of Silver Nanoparticles in Urban Wastewater Systems* Water Research, **47**, 12, 3866-3877, 2013
29. **Korablov, D., Ravnsbæk, D.B., Ban, V., Filinchuk, Y., Besenbacher, F., Jensen, T.R.** *Investigation of MBH4–VCl2, M = Li, Na or K* Int. J. Hydrogen Energy, **38**, 20, 8376–8383, 2013
30. **Korthout, K., Parmentier, A.B., Smet, Ph.F., Dirk, P.** *A XAS study of the luminescent Eu centers in thiosilicate phosphors* Phys. Chem. Chem. Phys., **15**, 8678-8683, 2013
31. **Leardini, L., Quartieri, S., Vezzalini, G., Martucci, A., Dmitriev, V.** *Elastic behavior and high pressure-induced phase transition in chabazite: new data from a natural sample from nova scotia* Microp.& Mesop. Mater., **170,** 52-61, 2013
32. **Leontyeva, D.V., Leontyev, I.N., Avramenko, M.V., Yuzyuk, Yu.I., Kukushkina, Yu.A., Smirnova, N.V.** *Electrochemical dispergation as a simple and effective technique toward preparation of NiO based nanocomposite for supercapacitor application* Electrochimica Acta, **114**, 356–362, 2013
33. **Liu, Y.-Y., Couck, S., Vandichel, M., Grzywa, M., Leus, K., Biswas, Sh., Volkmer, D. et al.** New VIV-Based Metal–Organic Framework Having Framework Flexibility and High CO2 Adsorption Capacity Inorg. Chem., **52**, 1, 113–120, 2013
34. **Lototskyy, M., Sibanyoni, J.M., Denys, R.V., Williams, M., Pollet B.G., Yartys, V.A.** *Magnesium-Carbon Hydrogen Storage Hybrid Materials Produced by Reactive Ball Milling in Hydrogen* Carbon, **57**, 146-160, 2013
35. **Lu, Y., Eyssler, A., Otal, E. H., Matam, S.K., Brunko, O., Weidenkaff, A., Ferri, D.** *Influence of the synthesis method on the structure of Pd-substituted perovskite catalysts for methane oxidation* Catalysis Today, **208**, 42-47, 2013

36. **Maehlen, J.P., Mongstad, T.T., You, Ch. Ch., Karazhanov S.** *Lattice contraction in photochromic yttrium hydride* J. Alloys and Compounds, **580**, 1, S119-S121, 2013
37. **Makarova, I. P., Grebenev, V. V., Chernaya, T. S., Verin, I. A. et al.** *Temperature-induced changes in the single-crystal structure of $K_9H_7(SO_4)_8 \cdot H_2O$* Crystallography Reports, **58**, 3, 393-400, 2013
38. **Michalow, K.A., Otal, E.H., Burnat, D., Fortunato, G., Emerich, H., Ferri, D., Heel, A. et al.** *Flame-made visible light active TiO2:Cr photocatalysts: Correlation between structural, optical and photocatalytic properties* Catalysis Today, **209**, 47-53, 2013
39. **Miller, S.R., Alvarez, E., Fradcourt, L., Devic, Th., Wuttke, S., Wheatley, P.S., Steunou, N., Bonhomme, Ch. et al.** *A rare example of a porous Ca-MOF for the controlled release of biologically active NO* Chem. Commun., **49**, 7773-7775, 2013
40. **Mondal, S., Van Smaalen, S., Parakhonskiy, G., Prathapa, S. J., Noohinejad, L., Bykova, E., Dubrovinskaia, N. et al.** *Experimental evidence of orbital order in α -B_{12} and γ-B_{28} polymorphs of elemental boron* Phys. Rev. B **88**, 024118-024126, 2013
41. **Moury, R., Demirci, U.B., Ichikawa, T., Filinchuk, Y., Chiriac, R., Van der Lee, A., Miele, Ph.** *Sodium Hydrazinidoborane: A Chemical Hydrogen-Storage Material* ChemSusChem, **6**, 4, 667-673, 2013
42. **Niehaus, O., Chevalier, B., Abdala, P.M., Winter, F., Pöttgen, R.** *The Solid Solutions (Ce1-xLax)RuSn* Z. Naturforsch., **68b**, 1279 – 1287, 2013
43. **Niehaus, O., Abdala, P.M., Riecken, J.F., Winter, F., Chevalier, B., Pöttgen, R.** *Cerium Valence Change in the Solid Solutions $Ce(Rh_{1-x}Ru_x)Sn$* Z. Naturforsch., **68b**, 960 – 970, 2013
44. **Nielsen, Th., Karkamkar, A., Bowden, M., Besenbacher, F., JensenT.R., Autrey, T.** *Methods to stabilize and destabilize ammonium borohydride* Dalton Trans., **42**, 680-687, 2013
45. **Nwakwuo, Ch. C., Holm, Th., Denys, R. V., Hu, W., Maehlen, J. P., Solberg, J. K., Yartys, V. A.** *Effect of magnesium content and quenching rate on the phase structure and composition of rapidly solidified La_2MgNi_9 metal hydride battery electrode alloy* J. Alloys & Compounds, **555**, 201–208, 2013
46. **Olsen, J.E., Frommen, Ch., Sørby, M.H., Hauback, B.C.** *Crystal structures and properties of solvent-free $LiYb(BH_4)_{4-x}Cl_x$, $Yb(BH_4)_3$ and $Yb(BH_4)_{2-x}Cl_x$* RSC Adv., **27,** 3, 10764-10774, 2013
47. **Ovsyannikov, S. V., Abakumov, A.M., Tsirlin, A.A., Schnelle, W., Egoavil, R., Verbeeck, J., Tendeloo, J.V. et al.** *Perovskite-like Mn2O3: A Path to New Manganites* Angewandte Chemie Int. Ed., **52**, 5, 1494-1498, 2013
48. **Parakhonskiy, G., Dubrovinskai, N., Bykova, E., Wirth, R., Dubrovinsky, L.** *High pressure synthesis and investigation of single crystals of metastable boron phases* High Pressure Research: Int. J., **33**, 3, 2013
49. **Paul, A.K., Jansen, M., Yan, B., Felser, C., Reehuis, M., Abdala, P.M.** *Synthesis, Crystal Structure, and Physical Properties of Sr_2FeOsO_6* Inorg. Chem., **52**, 11, 6713–6719, 2013
50. **Paul, A.K., Reehuis, M., Ksenofontov, V., Yan, B., Hoser, A., Többens, D.M., Abdala, P.M. et al.** *Lattice Instability and Competing Spin Structures in the Double Perovskite Insulator Sr_2FeOsO_6* Phys. Rev. Lett., **111**, 167205-167210, 2013
51. **Paul, A.K., Reehuis, M., Felser, C., Abdala, P.M., Jansen, M.** *Synthesis, Crystal Structure, and Properties of the Ordered Double Perovskite Sr_2CoOsO_6* Zeitschrift für anorganische und allgemeine Chemie, **639**, 14, 2421-2425, 2013
52. **Pekov, I. V., Chukanov, N. V., Filinchuk, Ya. E., Zadov, A. E., Kononkova, N. N. et al.** *Kasatkinite, $Ba_2Ca_8B_5Si_8O_{32}(OH)_3 \cdot 6H_2O_6$, a new mineral from the Bazhenovskoe deposit, the Central Urals, Russia* Geology of Ore Deposits, **55**, 7, 558-566, 2013
53. **Pekov, I. V., Zubkova, N. V., Chernyshov, D. Yu., Zelenski, M. E., Yapaskurt, V. O., Pushcharovskii, D. Yu**. *A new Cu-rich variety of lyonsite from fumarolic sublimates of the Tolbachik volcano (Kamchatka, Russia) and its crystal structure* Doklady Earth Sciences, **448**, 1, 112-116, 2013
54. **Peña, D., Griboval-Constant, A., Diehl, F., Lecocq, V., Khodakov, A.Y.** *Agglomeration at the Micrometer Length Scale of Cobalt Nanoparticles in Alumina-Supported Fischer–Tropsch Catalysts in a Slurry Reactor* ChemCatChem, **5**, 3, 728-731, 2013
55. **Pitt,M.P., Vullum, P.E., Sørby, M.H., Emerich, H., Paskevicius, M., Buckley, C.E. et al.** *Crystalline Al1 - x Ti x phases in the hydrogen cycled NaAlH4 + 0.02TiCl3 system* Philosophical Magazine, **93**, 9, 2013
56. **Popoff, N., Espinas, J., Pelletier, J., Macqueron, B., Szeto, K.C., Boyron, O. et al.** *Small Changes Have Consequences: Lessons from Tetrabenzyltitanium and -zirconium Surface Organometallic Chemistry* Chemistry - A European J., **19**, 3, 964–973, 2013

57. **Ravnsbæk, D. B., Nickels, E. A., Cerný, R., Olesen, C. H., David, W. I. F., Edwards, P. P., Filinchuk, Y., Jensen, T. R.** *Novel Alkali Earth Borohydride $Sr(BH_4)_2$ and Borohydride-Chloride $Sr(BH_4)Cl$* Inorg. Chem., **52**, 19, 10877–10885, 2013
58. **Røhr, A.K., Hammerstad, M., Andersson, K.K.** *Tuning of Thioredoxin Redox Properties by Intramolecular Hydrogen Bonds* PLOS ONE, **8**, 7, e69411, 2013
59. **Rozynek, Z., Zacher, T., Janek, M., Caplovicová, M., Fossum, O.J.** *Electric-field-induced structuring and rheological properties of kaolinite and halloysite* Applied Clay Science, **77-78**, 1-9, 2013
60. **Salamat, A., Hector, A.L., Gray, B.M.,Kimber, S.A.J., Bouvier, P., McMillan, P.F**. *Synthesis of Tetragonal and Orthorhombic Polymorphs of Hf3N4 by High-Pressure Annealing of a Prestructured Nanocrystalline Precursor* J. Am. Chem. Soc., **135**, 25, 9503–9511, 2013
61. **Sene, S., Reinholdt, M., Renaudin, G., Berthomieu, D., Zicovich-Wilson, C.M., Gervais, Ch., Gaveau, Ph.** *Boronate Ligands in Materials: Determining Their Local Environment by Using a Combination of IR/Solid-State NMR Spectroscopies and DFT Calculations* Chemistry - A European J., **19**, 3, 880–891, 2013
62. **Seryotkin, Y. V., Drebushchak, T.N., Boldyreva, E.V.** *A high-pressure polymorph of chlorpropamide formed on hydrostatic compression of the* α-form in saturated ethanol solution Acta Crystall., B **69**, 1, 77–85, 2013
63. **Šimuneková, M., Schwendt, P., Chrappová, J., Smrcok, L., Cerný, R., Van Beek, W.** *The first transition metal iodato peroxido complex: the synthesis, vibrational spectra and crystal structure from powder diffraction data of $K_3[V_2O_2(O_2)_4(IO_3)]\cdot H_2O$* Central Eur. J. Chemistry, **11**, 8, 1352-1359, 2013
64. **Smirnova, N. V., Kuriganova, A. B., Leont'eva, D. V., Leont'ev, I. N., Mikheikin, A. S.** *Structural and electrocatalytic properties of Pt/C and Pt-Ni/C catalysts prepared by electrochemical dispersion* Kinetics and Catalysis, **54**, 2, 255-262, 2013
65. **Sønsteby, H. H., Chernyshov, D., Getz, M., Nilsen, O., Fjellvåg, H.** *On the application of a single-crystal [kappa]-diffractometer and a CCD area detector for studies of thin films* J. Synchrotron Rad., **20**, 4, 2013
66. **Sønsteby, H. H., Østreng, E., Fjellvåg, H., Nilsen, O.** *Deposition and x-ray characterization of epitaxial thin films of $LaAlO_3$* Thin Solid Films, **550,** 90-94, 2013
67. **Subashini, A., Leela, S., Ramamurthi, K., Arakcheeva, A., Stoeckli-Evans, H., Petricek, V. et al.** *Synthesis, growth and characterization of 4-bromo-4'-nitrobenzylidene aniline (BNBA): a novel nonlinear optical material with a (3+1)-dimensional incommensurately modulated structure* CrystEngComm, **15**, 2474-2481, 2013
68. **Suwarno, S.., Solberg, J.K., Mæhlen, J.P., Denys, R.V., Krogh, B., Ochoa-Fernández, E. et al.** *Non-isothermal kinetics and in situ SR XRD studies of hydrogen desorption from dihydrides of binary Ti–V alloys* Int. J. Hydrogen Energy, **38**, 34, 14704-14714, 2013
69. **Svitlyk, V ., Chernyshov, D., Pomjakushina, E., Krzton-Maziopa, A., Conder, K., Pomjakushin, V. et al.** *Crystal structure of $BaFe_2Se_3$ as a function of temperature and pressure: phase transition phenomena and high-order expansion of Landau potential* J. Phys.: Condens. Matter., **25**, 315403-315413, 2013
70. **Svitlyk, V., Hermes, W., Chevalier, B., Matar, S.F., Gaudin, E., Voßwinkel, D., Chernyshov, D. et al.** *Change of the cerium valence with temperature – structure and chemical bonding of HT-CeRhGe* Solid State Sciences, **21**, 6-10, 2013
71. **Tagantsev, A. K. , Vaideeswaran, K., Vakhrushev, S. B., Filimonov, A. V., .Burkovsky, R. G., Shaganov, A. et al.** *The origin of antiferroelectricity in $PbZrO_3$* Nature Communications, **4**, 2229-2236, 2013
72. **Tchougréeff, A. L., Dronskowski, R.** *Low-temperature structure anomalies in CuNCN. Manifestations of RVB phase transitions?* J. Phys.: Condens. Matter, **25**, 435602-435625, 2013
73. **Tsakoumis, N.E., Dehghan, R., Johnsen, R.E., Voronov, A., Van Beek, W., Walmsley, J.S. et al.** *A combined in situ XAS-XRPD-Raman study of Fischer–Tropsch synthesis over a carbon supported Co catalyst* Catalysis Today, **205**, 86-93, 2013
74. **Tsypkin, M., Goméz de la Fuente, J.L., Rodríguez, S.G., Yua, Y., Ochal, P., Seland, F., Safonova, O. et al.** *Effect of heat treatment on the electrocatalytic properties of nano-structured Ru cores with Pt shells* J. Electroanalytical Chem., **704**, 57–66, 2013
75. **Wragg, D.S., Grønvold, A., Voronov, A., Norby, P., Fjellvåg, H.** *Combined XRD and Raman studies of coke types found in SAPO-34 after methanol and propene conversion* Microp.& Mesop. Mat., **173**, 166–174, 2013

76. **Wragg, D., O'Brien, M.G., Bleken, F., Fjellvåg, H., Di Michiel, M., Olsbye, U.** *The fast Z-scan method for studying working catalytic reactors with high energy X-ray diffraction: ZSM-5 in the methanol to gasoline process* Phys. Chem. Chem. Phys., **15**, 8662-8671, 2013

2014

1. **Abdala, P. M., Mauroy, H., Van Beek, W.** *A large-area CMOS detector for high-energy synchrotron powder diffraction and total scattering experiments* J. Appl. Cryst., **47**, 449-457, 2014
2. **Aboshyan-Sorgho, L., Lathion, T., Guénée, L., Besnard, C., Piguet, C.** *Thermodynamic N-Donor trans Influence in Labile Pseudo-Octahedral Zinc Complexes: A Delusion* Inorg. Chem., **53**, 24, 13093-13104, 2014
3. **Andreeva, N. V., Tyunina, M., Filimonov, A. V., Rudskoy, A. I., Pertsev, N. A., Vakhrushev, S. B.** *Low-temperature evolution of local polarization properties of $PbZr_{0.65}Ti_{0.35}O_3$ thin films probed by piezoresponse force microscopy* Appl. Phys. Lett., **104**, 112905-112912, 2014
4. **Arzac, G. M., Rojas-Ruiz, C., Gontard, L.C., Chinchilla, L.E., Otal, E.H., Crespo, P., Fernández, A.** *Chemistry, Nanostructure and Magnetic properties of Co-Ru-B-O Nanoalloys* RSC Adv., **4**, 46576-46586, 2014
5. **Ashok, A., Haavik, C., Norby, P., Norby, T., Olsen, A.** *Vacancy Ordering and Superstructure Formation in Dry and Hydrated Strontium Tantalate Perovskites: A TEM perspective* Micron, **62**, 11–27, 2014
6. **Alvaro-Muñoz, T., Pinar, A.B., Sisak, D., Perez-Pariente, J., Gómez-Hortigüela, L.** *Synthesis of the Aluminophosphate ICP-1 by Self-Assembly of 1,3-Diphenylguanidine: Insights into Supramolecular Aggregation* J. Phys. Chem. C, **118**, 9, 4835–4845, 2014
7. **Amirnasr, M., Bagheri, M., Farrokhpour, H., Schenk, K., Mereiter, K., Ford, P.C.** *New Zn(II) complexes with N_2S_2 Schiff base ligands. Experimental and theoretical studies of the role of Zn(II) in disulfide thiolate- exchange* Polyhedron, **71**, 1-7, 2014
8. **Arletti, R., Mugnaioli, E., Kolb, U., Di Renzo, F.** *MZ-35, a new layered pentasil borosilicate synthesized in the presence of large alkali cations* Microporous and Mesoporous Materials, **189**, 64–70, 2014
9. **Arletti, R., Vezzalini, G., Quartieri, S., Di Renzo, F., Dmitriev, V.** *Pressure-induced water intrusion in FER-type zeolites and the influence of extraframework species on structural deformations* Microp. & Mesop. Materials, **191**, 27–37, 2014
10. **Ban, V., Soloninin, A.V., Skripov, A.V., Hadermann, J., Abakumov, A.M., Filinchuk, Y.** *Pressure-Collapsed Amorphous Mg(BH4)2: An Ultra-dense Complex Hydride Showing a Reversible Transition to the Porous Framework* J. Phys. Chem. C, **118**, 40, 23402-23408, 2014
11. **Bellettato, M., Bonoldi, L., Cruciani, G., Flego, C., Guidetti, S., Millini, R., Montanari, E. et al.** *Flexible Structure of a Thermally Stable Hybrid Aluminosilicate Built with Only the Three-Ring Unit* J. Phys. Chem. C, **118**, 14, 7458–7467, 2014
12. **Bespalova, J. I., Khramenkova, A. V., Abdala, R. M., Dmitriev, V.P.** *Study of the Phase Composition and Structure of Composite Coatings Based on TransitionMetal Oxide Compounds via XRay Diffraction and Xray Absorption Fine Structure Spectroscopy* J. Surface Investigation. Xray, Synchrotron and Neutron Tech., **8**, 1, 60-65, 2014
13. **Blazina, T., Sun, Y., Voegelin, A., Lenz, M., Berg, M., Winkel, L.H.E**. *Terrestrial selenium distribution in China is potentially linked to monsoonal climate* Nature Communications, **5**, Article number: 4717, 2014
14. **Bosak, A., Chernyshov, D., Hoesch, M., Piekarz, P., Le Tacon, M., Krisch, M. et al.** *Short-Range Correlations in Magnetite above the Verwey Temperature* Phys. Rev. X, **4**, 011040 – 011047, 2014
15. **Bouhoute, Y., Garron, A., Grekov, D., Merle, N., Szeto, K.Ch., De Mallmann, A., Rosal, I.D., Maron, I., Girard, G. et al.** *Well-defined supported mononuclear tungsten oxo species as olefin metathesis pre-catalysts* ACS Catalysis, **4**, 11, 4232-4241, 2014
16. **Bøyesen, K.L., Kristiansen, T., Mathisen, K.** *Identification of Synergistic Cu/V Red-ox Pair in VCu:AlPO-5; a Comparison with VCu:ZSM-5* Phys. Chem. Chem. Phys., **16**, 20451-20463, 2014

17. **Bøyesen, K.L., Mathisen, K.** *Exposing the synergistic effect between copper and vanadium in AlPO-5 during the selective oxidation of propene* Catalysis Today, **229**, 14–22, 2014
18. **Bras, W., Stanley, H.B., Banerjee, D., Merino, D.H., Longo, A., Portale, G., Ciston, J. et al.** *X-ray Irradiation Induced Reduction and Nanoclustering of Lead in a Borosilicate Glass* CrystEngComm, **16**, 9331-9339, 2014
19. **Bugaev, A.L., Guda, A.A., Lomachenko, K.A., Srabionyan, V.V., Bugaev, L.A., Soldatov, A.V., Lamberti, C. et al.** *Temperature- and Pressure-Dependent Hydrogen Concentration in Supported PdHx Nanoparticles by Pd K-Edge X-ray Absorption Spectroscopy* J. Phys. Chem. C, **118**, 19, 10416-10423, 2014
20. **Burkovsky, R. G., Tagantsev, A. K., Vaideeswaran, K., Setter, N., Vakhrushev, S. B., Filimonov, A. V., Shaganov, A., Andronikova, D. et al.** *Lattice dynamics and antiferroelectricity in $PbZrO_3$ tested by x-ray and Brillouin light scattering* Phys. Rev. B **90**, 144301-144313, 2014
21. **Cano, I., Chapman, A.M., Urakawa, A., Van Leeuwen, P. W. N. M.** *Air-Stable Gold Nanoparticles Ligated by Secondary Phosphine Oxides for the Chemoselective Hydrogenation of Aldehydes: Crucial Role of the Ligand* J. Am. Chem. Soc., **136,** 6, 2520–2528, 2014
22. **Carrington, E. J., Vitorica-Yrezabal, I. J., Brammer, L.** *Crystallographic studies of gas sorption in metal-organic frameworks* Acta Cryst., B**70**, 404-422, 2014
23. **Chakraborty, P., Enachescu, C., Humair, A., Egger, L., Delgado, T., Tissot, A., Guénée, L. et al.** *Light-induced spin-state switching in the mixed crystal series of the 2D coordination network $\{[Zn_{1-x}Fe_x(bbtr)_3](BF_4)_2\}_\infty$: optical spectroscopy and cooperative effects* Dalton Trans., **43**, 17786-17796, 2014
24. **Chambrier, M.- H., Le Bail, A., Giovannelli, F., Redjaïmia, A., Florian, P., Massiot, D. et al.** *$La_{10}W_2O_{21}$: An Anion-Deficient Fluorite-Related Superstructure with Oxide Ion Conduction* Inorg. Chem., **53**, 1, 147–159, 2014
25. **Chernyshov, D., Dyadkin, V., Dmitriev, V., Bossak, A.** *Pressure evolution of $PbMg_{1/3}Nb_{2/3}O_3$ relaxor ferroelectric* Zeitschrift für Kristallographie – Crystalline Materials, **229**, 3, 223–229, 2014
26. **Christensen, A.N., Lebech, B., Andersen, N.H., Grivel, J.C.** *Crystal structure of paramagnetic copper (II) oxalate (CuC2O4): Formation and thermal decomposition of randomly stacked anisotropic nano-sized crystallites* Dalton Trans., **43**, 16754-16768, 2014
27. **Chumakova, A.V., Valkovskiy, G.A., Mistonov, A.A., Dyadkin, V.A., Grigoryeva, N.A., Sapoletova, N.A., Napolskii, K.S. et al.** P*eriodic order and defects in Ni-based inverse opal-like crystals on the mesoscopic and atomic scale* Phys. Rev. B **90**, 144103-144112, 2014
28. **Dilnesa, B.Z., Lothenbach, B., Renaudin, G., Wichser, A., Kulik, D.** *Synthesis and characterization of hydrogarnet $Ca_3(Al_xFe_{1-x})2(SiO_4)_y(OH)_{4(3-y)}$* Cement and Concrete Res., **59**, 96–111, 2014
29. **Doronkin, D.E., Fogel, S., Gabrielsson, P., Grunwaldt, J.-D., Dahl, S.** *Ti and Si doping as a way to increase low temperature activity of sulfated Ag/Al_2O_3 in H_2-assisted NH_3-SCR of NO_x* Applied Catalysis B: Environmental, **148–149**, 62–69, 2014
30. **Dovgaliuk, I., Ban, V., Sadikin, Y., Cerný, R., Aranda, L., Casati, N., Devillers, M., Filinchuk, Y.** *The First Halide-Free Bimetallic Aluminum Borohydride: Synthesis, Structure, Stability, and Decomposition Pathway* J. Phys. Chem. C, **118**, 1, 145–153, 2014
31. **Dovgaliuk, I., Hagemann, H., Leyssens, T., Devillers, M., Filinchuk, Y.** *CO_2-promoted hydrolysis of KBH4 for efficient hydrogen co-generation* Int. J. Hydrogen Energy, **39**, 34, 19603-19608, 2014
32. **Dyadkin, V., Grigoriev, S., Ovsyannikov, S. V., Bykova, E., Dubrovinsky, L., Tsvyashchenko, A. et al.** *Crystal structure and thermal expansion of $Mn_{1-x}Fe_xGe$* Acta Cryst., B**70**, 676-680, 2014
33. **Dyadkin, V., Prša, K., Grigoriev, S. V., White, J. S., Huang, P., Rønnow, H. M., Magrez, A. et al**. *Chirality of structure and magnetism in the magnetoelectric compound Cu_2OSeO_3* Phys. Rev. B **89**, 140409-140414, 2014
34. **Ehlert, K., Mikutta, Ch., Kretzschmar, R.** *Impact of Birnessite on Arsenic and Iron Speciation during Microbial Reduction of Arsenic-Bearing Ferrihydrite* Environ. Sci. Technol., **48**, 19, 11320-11329, 2014
35. **Emami, S., Paz, F.A.A., Mendes, A., Gales, L.** *Toward the Construction of 3D Dipeptide–Metal Frameworks* Cryst. Growth Des., **14**, 9, 4777-4780, 2014
36. **Filinchuk Y., Tumanov, N.A., Ban, V., Ji, H., Wei, J., Swift, M.W., Nevidomskyy, A.H., Natelson, D.** *In situ diffraction study of catalytic hydrogenation of VO_2: Stable phases and origins of metallicity* J. Am. Chem. Soc., **136**, 22, 8100-8109, 2014

37. **Galvita, V.V., Filez, M., Poelman, H., Bliznuk, V., Marin, G.B.** *The Role of Different Types of CuO in CuO–CeO_2/Al_2O_3 for Total Oxidation* Catalysis Letters, **144**, 32-43, 2014
38. **Gianotti, V., Favaro, G., Bonandini, L., Palin, L., Croce, G., Boccaleri, E., Artuso, E., Van Beek, W. et al.** *Rationalization of dye uptake on TiO_2 slides for Dye-sensitized Solar Cells by a combined chemometric and structural approach* ChemSusChem (CHEMSUSCHEM), 7, 11, 3039-3052, 2014
39. **Gigli, L., Arletti, A., Tabacchi, G., Fois, E., Vitillo, J.G., Martra, G., Agostini, G. et al.** *Close-Packed Dye Molecules in Zeolite Channels Self Assemble into Supramolecular Nanoladders* J. Phys. Chem. C, **118**, 29, 15732-15743, 2014
40. **Griboval-Constant, A., Butel, A., Ordomsky, V.V., Chernavskii, P.A., Khodakov, A.Y.** *Cobalt and iron species in alumina supported bimetallic catalysts for Fischer-Tropsch reaction* Applied Catalysis A: General, **481**, 116-126, 2014
41. **Grigoriev, S. V., Potapova, N. M., Moskvinm E. V., Dyadkin, V. A., Dewhurst, Ch., Maleyev, S. V.** *Hexagonal spin structure of A-phase in MnSi: densely packed skyrmion quasiparticles or two-dimensionally modulated spin superlattice?* JETR Letters, **100**, 3, 238 – 243, 2014
42. **Grove, H., Rude, L., Jensen, T.R., Corno, M., Ugliengo, P., Baricco, M., Sørby, M.S., Hauback, B.C.** *Halide substitution in $Ca(BH_4)_2$* RSC Adv., **4**, 4736-4742, 2014
43. **Hirsch, O., Zeng, G., Luo, L., Staniuk, M., Abdala, P.M., Van Beek, W., Rechberger, F. et al.** *Aliovalent Ni in MoO_2 Lattice— Probing the Structure and Valence of Ni and Its Implication on the Electrochemical Performance* Chem. Mater., **26**, 15, 4505-4513, 2014
44. **Humphries, T.D., Makepeace, J.W., Hino, H., David, B., Hauback, B.C.** *Regeneration of Sodium Alanate studied by powder in situ neutron and synchrotron X-ray diffraction* J. Mater. Chem. A, **2**, 16594-16600, 2014
45. **Jensen, A.Ch.S., Ibsen, C., Sutherland, D.S., Birkedal. H.** *Transparent aggregates of nanocrystalline hydroxyapatite* Cryst. Growth Des., **14**, 12, 6343-6349, 2014
46. **Jepsen, L. H., Ban, V., Møller, K.T., Lee, Y.-S., Cho, Y.W., Besenbacher, F., Filinchuk, Y., Skibsted, J.** *Synthesis, Crystal Structure, Thermal Decomposition and ^{11}B MAS NMR Characterization of $Mg(BH_4)_2(NH_3BH_3)_2$* J. Phys. Chem. C, **118**, 23, 12141-12153, 2014
47. **Jepsen, L. H., Ravnsbæk, D. B., Grundlach, C., Besenbacher, F., Skibstede, J., Jensen, T. R.** *A novel intermediate in the $LiAlH_4$–$LiNH_2$ hydrogen storage system* Dalton Trans., **43**, 3095-3103, 2014
48. **Kalantzopoulos, G.N., Guzik, M.N., Deledda, S., Heyn, R.H., Mullera, J., Hauback, B.C.** *Destabilization effect of transition metal fluorides on sodium borohydride* Phys. Chem. Chem. Phys., **16**, 20483-20491, 2014
49. **Kochur, A.G., Kozakov, A.T., Googlev, K.A., Mikheykin, A.S., Torgashev, V.I., Bush, A.A., Nikolskii, A.V.** *Chemical bonding and valence state of 3d-metal ions in $Ni_{1-x}Co_xCr_2O_4$ spinels from X-ray diffraction and X-ray photoelectron spectroscopy data* J. Electr. Spectroscopy & Related Phenomena, **195**, 208-219, 2014
50. **Kranzlin, N., Staniuk, M., Heiligtag, F. J., Luo, L., Emerich, H., Van Beek, W., Niederbergera, M., Koziej, D.** *Rationale for the crystallization of titania polymorphs in solution* Nanoscale, **6**, 14716-14723, 2014
51. **Kristiansen, T., Mathisen, K.** *On the Promoting Effect of Water during NO_x Removal over Single-Site Copper in Hydrophobic Silica APD-Aerogels* J. Phys. Chem. C, **118,** 5, 2439–2453, 2014
52. **Kroll, A., Behra, R., Kaegi, R., Sigg, L.** *Extracellular Polymeric Substances (EPS) of Freshwater Biofilms Stabilize and Modify CeO_2 and Ag Nanoparticles* PLOS ONE, **9** , 10, 110709-110725, 2014
53. **Kuczera, P., Wolny, J., Steurer, W.** *High-temperature structural study of decagonal Al-Cu-Rh* Acta Cryst., B**70**, 306-314, 2014
54. **Leontyev, I. N., Kuriganova, A. B., Leontyev, N. G., Hennet, L., Rakhmatullin, A., Smirnova, N. V., Dmitriev, V.** *Size dependence of the lattice parameters of carbon supported platinum nanoparticles: X-ray diffraction analysis and theoretical considerations* RSC Adv., **4**, 35959-35965, 2014
55. **Ley, M.B., Paskevicius, M., Schouwink, P., Richter, B., Sheppard, D.A., Buckley, C.E., Jensen, T.R.** *Novel solvates $M(BH_4)_3S(CH_3)_2$ and properties of halide-free $M(BH_4)_3$ (M = Y or Gd)* Dalton Trans., **43**, 13333-13342, 2014
56. **Leyssens, T., Tumanova, N., Robeyns, K., Candonib, N., Veesler, S.** *Solution cocrystallization, an effective tool to explore the variety of cocrystal systems: caffeine/dicarboxylic acid cocrystals* CrystEngComm, **16**, 9603-9611, 2014

57. **Logvinovich, D., Simonov, A., Steurer, W.** *Structure of decagonal Al-Ni-Rh* Acta Cryst., B**70**, 732-742, 2014
58. **Makarova, I., Grebenev, V., Dmitricheva, E., Dolbinina, V., Chernyshov, D.** *$M_mH_n(XO_4)_{(m+n)/2}$ crystals: structure, phase transitions, hydrogen bonds, conductivity. I. $K_9H_7(SO_4)_8 \cdot H_2O$ crystals - a new representative of the family of solid acid conductors* Acta Cryst., B**70**, 218-226, 2014
59. **Mandaliev, P.N., Mikutta, Ch., Barmettler, K., Kotsev, T., Kretzschmar, R.** *Arsenic Species Formed from Arsenopyrite Weathering along a Contamination Gradient in Circumneutral River Floodplain Soils* Environ. Sci. Technol., **48**, 1, 208–217, 2014
60. **Marchiori, Ch., Liberto, G.D., Soliveri, G., Loconte, L., Presti, L.L., Meroni, D., Ceotto, M., Oliva, C. et al.** *Unraveling the Cooperative Mechanism of Visible-Light Absorption in Bulk N,Nb Codoped TiO_2 Powders of Nanomaterials* J. Phys. Chem. C, **118**, 41, 24152-24164, 2014
61. **Mendes, P.A.P., Horcajada, P., Rives, S., Ren, H., Rodrigues, A.E., Devic, Th., Magnier, E., Trens, Ph., Jobic, E., Ollivier, J. et al**. *A Complete Separation of Hexane Isomers by a Functionalized Flexible Metal Organic Framework* Advanced Functional Materials, **24**, 48, 7666-7673, 2014
62. **Mikheykin, A. S., Chernyshov, D. Yu., Bush, A. A., Prokhorov, A. S., Yuzyuk, Yu. I., Dmitriev, V. P.** *Features of the Jahn-Teller transition in $Ni_{1-x}Co_xCr_2O_4$ solid solutions* Physics of the Solid State, **56**, 4, 785-791, 2014
63. **Mikheykin, A. S., Torgashev, V.I., Talanov, V. M. , Bush, A A., Chernyshov, D., Yuzyuk, Yu.I., Dmitriev, V P.** *High pressure x-ray diffraction study of nickel–copper chromites solid solutions* J. Phys.: Condens. Matter, **26**, 505401-505409, 2014
64. **Mikutta, Ch., Mandaliev, P.N., Mahler, N., Kotsev, T., Kretzschmar, R.** *Bioaccessibility of Arsenic in Mining-Impacted Circumneutral River Floodplain Soils* Environ. Sci. Technol., **48**, 22, 13468-13477, 2014
65. **Møller, K.T., Hansen, B.R.S., Dippel, A.-Ch., Jørgensen, J.E., Jensen, T.R.** *Characterization of Gas-Solid Reactions using In Situ Powder X-ray Diffraction* ZAAC, **640**, 15, 3029-3043, 2014
66. **Morozov, V.A., Raskina, M.V., Lazoryak, B.I., Meert, K.W., Korthout, K., Smet, Ph.F., Poelman, D., Gauquelin, N. et al.** *Crystal Structure and Luminescent Properties of R2-xEux(MoO4)3 (R=Gd, Sm) Red Phosphors* Chem. Mater., **26**, 24, 7124-7136, 2014
67. **Moulin, B., Salles, F., Bourrelly, S., Llewellyn, Ph.L., Devic, Th., Horcajada, P., Serre, Ch. et al.** *Effect of the ligand functionalization on the acid–base properties of flexible MOFs* Microporous and Mesoporous Materials, **195**, 197–204, 2014
68. Moury, R., Demirci, U. B., Ban, V., Filinchuk, Y., Ichikawa, T., Zeng, L., Goshome, K., Miele, Ph. *Lithium hydrazinidoborane, a polymorphic material with potential for chemical hydrogen storage* Chem. Mater., **26**, 10, 3249-3255, 2014
69. **Nallamuthu, S., Rashid, T.P., Krishnakumar, V., Besnard, C., Hagemann, H., Reiffers, M., Nagalakshmi, R.** *Anisotropic magnetic, transport and thermodynamic properties of novel tetragonal Ce_2RhGa_{12} compound* J. Alloys & Compounds, **604**, 379–383, 2014
70. **Niehaus, O., Rodewald, U.Ch., Abdala, P.M., Touzani, R.St.., Fokwa, B. P. T., Janka, O.** *Synthesis and Theoretical Investigations of the Solid Solution $CeRu_{1-x}Ni_xAl$ (x = 0.1–0.95) Showing Cerium Valence Fluctuations* Inorg. Chem., **53**, 5, 2471-2480, 2014
71. **Olsen, J.E., Frommen, Ch., Jensen, T.R., Riktor, M.D., Sørby, M.H., Hauback, B.S.** *Structure and thermal properties of composites with RE-borohydrides (RE = La, Ce, Pr, Nd, Sm, Eu, Gd, Tb, Er, Yb or Lu) and $LiBH_4$* RSC Adv., **4,** 1570-1582, 2014
72. **Olsen, J.E., Karen, P., Sørby, M.H., Hauback, B.S.** *Effect of chloride substitution on the order–disorder transition in $NaBH_4$ and $Na^{11}BD_4$* J. Alloys & Compounds, **587**, 374–379, 2014
73. **Ors, T., Takakura, H., Abe, E., Steurer, W.** *The quasiperiodic average structure of highly disordered decagonal Zn-Mg-Dy and its temperature dependence* Acta Cryst., B**70**, 315-330, 2014
74. **Ovsyannikov, S.V., Gou, H., Karkin, A.E., Shchennikov, V.V., Wirth, R., Dmitriev, V.P., Nakajima, Y. et al.** *Bulk Silicon Crystals with the High Boron Content, Si1-xBx: Two Semiconductors Form an Unusual Metal* Chem. Mater., **26**,18, 5274-5281, 2014
75. **Panahian Jand, S., Kaghazchi, P.** *The role of electrostatic effects in determining the structure of LiF-graphene interfaces* J. Phys.: Condens. Matter, **26**, 262001-262008, 2014
76. **Postnikov, V.A., Odarchenko, Y., Iovlev, A.V., Bruevich, V.V., Pereverzev, A.Y., Kudryashova, L.G., Sobornov, V.V. et al.** *Molecularly-smooth single-crystalline films of*

thiophene-phenylene co-oligomers grown at the gas-liquid interface Cryst. Growth Des., **14**, 4, 1726–1737, 2014

77. **Presti, L.L., Ceotto, M., Spadavecchia, F., Cappelletti, G., Meroni, D., Acres, R.G., Ardizzone, S.** *Role of the Nitrogen Source in Determining Structure and Morphology of N-Doped Nanocrystalline TiO_2* J. Phys. Chem. C, **118**, 9, 4797–4807, 2014
78. **Regelink, I., Voegelin, A., Weng, L.L., Koopmans, G.F., Comans, R.N.J.** *Characterization of Colloidal Fe from Soils using Field-Flow Fractionation and Fe K-edge X-ray Absorption Spectroscopy* Environ. Sci. Technol., **48**, 8, 4307–4316, 2014
79. **Safonova, O. V. , Guda, A. A., Paun, C., Smolentsev, N., Abdala, P. M., Smolentsev, G., Nachtegaal, M., Szlachetko, J., Soldatov, M. A. et al.** *Electronic and Geometric Structure of Ce^{3+} Forming Under Reducing Conditions in Shaped Ceria Nanoparticles Promoted by Platinum* J. Phys. Chem. C, **118**, 1974-1982, 2014
80. **Salvadó, N., Butí, S., Aranda, M.A.G., Pradell, T.** *New insights on blue pigments used in 15th century paintings by synchrotron radiation-based micro-FTIR and XRD* Anal. Methods, **6,** 3610-3621, 2014
81. **Schouwink, P., Ley, M.B., Jensen, T.R., Smrcok, L., Cerny, R.** *Borohydrides: From Sheet to Framework Topologies* Dalton Transactions, **43**, 7726-7733, 2014
82. **Schouwink, P., Ley, M.B., Tissot, A., Hagemann, H., Jensen, T.R., Smrcok, L., Cerný, R.** *Structure and properties of complex hydride perovskite materials* Nature Communications, **5**, 5706-5736, 2014
83. **Schouwink, P., Smrcok, L., Cerný, R.** *Role of the Li+ node in the Li-BH_4 substructure of double-cation tetrahydroborates* Acta Cryst., B**70**, 871-878, 2014
84. **Schuh, K., Kleist, W., Høj, M., Trouillet, V., Jensen, A.D., Grunwaldt, J.-D.** *One-step synthesis of bismuth molybdate catalysts via flame spray pyrolysis for the selective oxidation of propylene to acrolein* Chem. Commun., **50**, 15404-15406, 2014
85. **Sharafutdinov, I., Elkjær, Ch.F., Pereira de Carvalho, H.W., Gardini, D., Chiarello, G.L., Damsgaard, Ch.D., Wagner, J.B. et al.** I*ntermetallic compounds of Ni and Ga as catalysts for the synthesis of methanol* J. Catalysis, **320**, 77–88, 2014
86. **Shtender, V.V., Denys, R.V., Paul-Boncour, V., Riabov, A.B., Zavaliy, I.Yu.** *Hydrogenation properties and crystal structure of $YMgT_4$ (T=Co, Ni, Cu) compounds* J. Alloys & Compounds, **603,** 7–13, 2014
87. **Simonov, A., Weber, T., Steurer, W.** *Experimental uncertainties of three-dimensional pair distribution function investigations exemplified on the diffuse scattering from a tris-tert-butyl-1,3,5-benzene tricarboxamide single crystal* J. Appl. Cryst., **47**, 2011-2018, 2014
88. **Slawinski, W.A., Wragg, D.S., Akporiaye, D., Fjellvåg, H.** *Intergrowth structure modelling in silicoaluminophosphate SAPO-18/34 family* Microporous and Mesoporous Materials, **195**, 311-318, 2014
89. **Smeets, S., Xie, D., Baerlocher, Ch., McCusker, L.B., Wan, W., Zou, X., Zones, S.I.** *High-Silica Zeolite SSZ-61 with Dumbbell-Shaped Extra-Large-Pore Channels* Angewandte Chemie, **126**, 39, 10566-10570, 2014
90. **Sønsteby, H.H., Østreng, E., Fjellvåg, H., Nilsen, O.** *Deposition and x-ray characterization of epitaxial thin films of $LaAlO_3$* Thin Solid Films, **550**, 90–94, 2014
91. **Staniuk, M., Hirsch, O., Kränzlin, N., Böhlen, R., Van Beek, W., Abdala, P.M., Koziej, D.** *Puzzling Mechanism behind a Simple Synthesis of Cobalt and Cobalt Oxide Nanoparticles: In Situ Synchrotron X-ray Absorption and Diffraction Studies* Chem. Mater., **26**, 6, 2086–2094, 2014
92. **Sveinbjörnsson, D., Blanchard, D., Myrdal, J.S.G., Younesi, R., Viskinde, R., Riktor, M.D., Norby, P. et al.** *Ionic conductivity and the formation of cubic CaH_2 in the $LiBH_4$–$Ca(BH_4)_2$ composite* J. Solid State Chemistry, **211**, 81–89, 2014
93. **Svitlyk, V., Chernyshov, D. , Bosak, A., Pomjakushina, E. , Krzton-Maziopa, A., Conder, K. , Pomjakushin, V. , Dmitriev, V. et al.** *Compressibility and pressure-induced disorder in superconducting phase-separated $Cs_{0.72}Fe_{1.57}Se_2$* Phys. Rev. B **89**, 144106-144116, 2014
94. **Suwarno, S., Solberg, J.K., Maehlen, J.P., Krogh, B. Yartys, V.A.** The Effects of Rapid Solidification on Microstructure and Hydrogen Sorption Properties of Binary Bcc Ti-V Alloys J. Alloys & Compounds, **582**, 540-546, 2014
95. **Teteruk, J. L., Glinnemann, J., Gorelik, T. E., Linden, A., Schmidt, M. U.** *Explanation of the stacking disorder in the [beta]-phase of Pigment Red 170* Acta Cryst., B**70**, 296-305, 2014
96. **Thalmann, B., Voegelin, A., Sinnet, B., Morgenroth, E., Kaegi, R.** *Sulfidation Kinetics of Silver Nanoparticles Reacted with Metal Sulfides* Environ. Sci. Technol., **48**, 9, 4885-4892, 2014

97. **Thorkildsen, G., Larsen, H. B.** *Crystallography of embedded particles in Al-Mg-Zn alloys. Symmetry analysis* J. Appl. Cryst., **47**, 1736-1748 , 2014
98. **Tsakoumis, N.E., Dehghan-Niri, R., Ronning, M., Walmsley, J.S., Borg, O., Rytter, E., Holmen, A.** *X-ray absorption, X-ray diffraction and electron microscopy study of spent cobalt based catalyst in semi-commercial scale Fischer-Tropsch synthesis* Applied Catalysis A: General, **479**, 59-69, 2014
99. **Tumanova, N., Tumanov, N., Robeyns, K., Filinchuk, Y., Wouters, J., Leyssen, T.** *Structural insight into cocrystallization with zwitterionic co-formers: cocrystals of S-naproxen* CrystEngComm, **16**, 8185-8196, 2014
100. **Tyrsted, C., Lock, N., Jensen, K. M. Ø., Christensen, M., Bøjesen, E. D., Emerich, H., Vaughan, G. et al.** *Evolution of atomic structure during nanoparticle formation* IUCrJ, **1**, 3, 165-171, 2014
101. **Tyvanchuk, Y., Svitlyk, V., Pustovoychenko, M., Kalychak, Y.** *The crystal structure of $Sm_4Ni_{11}In_{20}$ and its relation to other indium-rich compounds* Central European J. Chem., **12**, 2, 227-232, 2014
102. **Voegelin, A., Kaegi, R., Berg, A.M., Nitzsche, K.S., Kappler, A., Lan, V.M., Trang, Ph.Th.K., Göttlicher, J., Steininger, R.** *Solid-phase characterisation of an effective household sand filter for As, Fe and Mn removal from groundwater in Vietnam* Environmental Chemistry, **11**, 5, 566-578
103. **Voronov, A., Tsakoumis, N.E., Hammer, N., Van Beek, W., Emerich, H., Rønning, M.** *The state and location of Re in Co–Re/Al_2O_3 catalysts during Fischer–Tropsch synthesis: Exploring high-energy XAFS for in situ catalysts characterisation* Catalysis Today, **229**, 23–33, 2014
104. **Voronov, A., Urakawa, A., Van Beek, W., Tsakoumis, N.E., Emerich, H., Rønning, M.** *Multivariate curve resolution applied to in situ X-ray absorption spectroscopy data: An efficient tool for data processing and analysis* Analytica Chimica Acta, **840**, 20, 20-27, 2014
105. **Warshamanage, R., Linden, A., Schmidt, M. U., Bürgi, H.-B.** *Average structures of the disordered [beta]-phase of Pigment Red 170: a single-crystal X-ray diffraction study* Acta Cryst., B**70**, 283-295, 2014
106. **Weber, Th.** *Crystallography beyond the Bragg Peaks* CHIMIA Int. J. Chemistry, **68,** 1, 60-65, 2014
107. **Wehinger, B., Bosak, A., Piccolboni, D., Refson, K., Chernyshov, D., Ivanov, A. et al.** *Diffuse scattering in metallic tin polymorphs* J. Phys.: Condens. Matter, **26**, 115401-115411, 2014
108. **Wehinger B., Chernyshov, D., Krisch, M., Bulat, S., Ezhov. V., Bosak, A**. *Diffuse scattering in Ih ice* J. Phys.: Condens. Matter, **26**, 265401-265411, 2014
109. **Wu, Q., Duchstein, L.D.L., Chiarello, G.L., Christensen, J.M., Damsgaard, Ch.D., Elkjær, C.F.** I*n Situ Observation of Cu–Ni Alloy Nanoparticle Formation by X-Ray Diffraction, X-Ray Absorption Spectroscopy, and Transmission Electron Microscopy: Influence of Cu/Ni Ratio* ChemCatChem, **6,** 1, 301–310, 2014